

University of Groningen

Neurodevelopment, brain vasculature and schizophrenia

Puvogel Lütjens, Sofía

DOI:
[10.33612/diss.582204366](https://doi.org/10.33612/diss.582204366)

IMPORTANT NOTE: You are advised to consult the publisher's version (publisher's PDF) if you wish to cite from it. Please check the document version below.

Document Version
Publisher's PDF, also known as Version of record

Publication date:
2023

[Link to publication in University of Groningen/UMCG research database](#)

Citation for published version (APA):

Puvogel Lütjens, S. (2023). *Neurodevelopment, brain vasculature and schizophrenia*. [Thesis fully internal (DIV), University of Groningen]. University of Groningen. <https://doi.org/10.33612/diss.582204366>

Copyright

Other than for strictly personal use, it is not permitted to download or to forward/distribute the text or part of it without the consent of the author(s) and/or copyright holder(s), unless the work is under an open content license (like Creative Commons).

The publication may also be distributed here under the terms of Article 25fa of the Dutch Copyright Act, indicated by the "Taverne" license. More information can be found on the University of Groningen website: <https://www.rug.nl/library/open-access/self-archiving-pure/taverne-amendment>.

Take-down policy

If you believe that this document breaches copyright please contact us providing details, and we will remove access to the work immediately and investigate your claim.

Downloaded from the University of Groningen/UMCG research database (Pure): <http://www.rug.nl/research/portal>. For technical reasons the number of authors shown on this cover page is limited to 10 maximum.



Chapter 3

Altered resting-state functional connectivity in hiPSCs-derived neuronal networks from schizophrenia patients

Sofia Puvogel^{1,2*}, Kris Blanchard^{1,2*}, Bárbara S. Casas¹, Robyn L. Miller^{3,4}, Delia Garrido-Jara¹, Sebastián Arizabalos¹, Stevens K. Rehen⁵, Magdalena Sanhueza^{2**}, Verónica Palma^{1**}

*, **: these authors contributed equally

¹Laboratory of Stem Cells and Developmental Biology, Department of Biology, Faculty of Sciences. Universidad de Chile. Santiago, Chile.

²Cell Physiology Laboratory, Department of Biology, Faculty of Sciences, Universidad de Chile, Santiago, Chile.

³Georgia State University, Dept of Computer Science, Atlanta GA, USA.

⁴Tri-institutional Center for Translational Research in Neuroimaging and Data Science (TReNDS Center), Atlanta, GA, USA.

⁵Instituto D'Or de Pesquisa e Ensino (IDOR), Rio de Janeiro, Brazil.

Abstract

Schizophrenia is a severe mental disorder that arises from abnormal neurodevelopment, caused by genetic and environmental factors. Schizophrenia often involves distortions in reality perception and it is widely associated with alterations in brain connectivity. In the present work, we used Human Induced Pluripotent Stem Cells (hiPSCs)-derived neuronal cultures to study neural communicational dynamics during early development in schizophrenia. We conducted gene and protein expression profiling, calcium imaging recordings, and applied a mathematical model to quantify the dynamism of functional connectivity (FC) in hiPSCs-derived neuronal networks. Along the neurodifferentiation process, schizophrenia networks displayed altered gene expression of the glutamate receptor-related proteins *HOMER1* and *GRIN1* compared to healthy control networks, suggesting a possible tendency to develop hyper-excitability. Resting-state FC in neuronal networks derived from healthy controls and schizophrenia patients emerged as a dynamic phenomenon exhibiting connectivity configurations reoccurring in time (hub states). Compared to healthy controls, schizophrenia networks were less thorough in exploring different FC configurations, changed configurations less often, presented a reduced repertoire of hub states, and spent longer uninterrupted time intervals in this less diverse universe of hubs. Our results suggest that alterations in the communicational dynamics of schizophrenia emerging neuronal networks might contribute to the previously described brain FC anomalies in schizophrenia patients, by compromising the ability of their neuronal networks for rapid and efficient reorganization through different activity patterns.

Introduction

Schizophrenia is a chronic mental disorder that affects over 20 million people worldwide [1]. The neurodevelopmental hypothesis of schizophrenia proposes that an abnormal developmental trajectory converges into vulnerable brain circuits, leading the organism prone to an increased likelihood of developing psychosis when faced with stressful events during adulthood [2]. Nonetheless, the mechanisms triggering and predicting the evolution of the disease remain poorly understood.

Different studies associate schizophrenia symptomatology with altered communication across different brain regions (reviewed in [3]). In this context, functional connectivity (FC) analysis, which calculates the temporal correlation between spatially remote events of brain activity, has been widely used to evaluate communication across the brain. One of the most common techniques used to measure regional brain activity is functional magnetic resonance imaging (fMRI) [4], which registers the hemodynamic variation in response to changes in brain activity. This methodology allows quantifying the temporal correlation between signals originating from different parcellated brain nodes (voxels); a measure that reflects how strongly different brain regions communicate. fMRI studies have shown abnormal brain FC in schizophrenia patients in both resting-state [5-8] and during task performance [6, 7, 9]. Some of the resting-state studies assumed that FC remains static during the data acquisition time period (~5-15 min) [10]; however, it has been demonstrated that brain resting-state FC is a non-stationary phenomenon. Instead, it characterizes by exploring different connectivity states [11, 12]. Furthermore, the flow-through of these configurations is not an arbitrary process, since discrete connectivity states consistently recur along with the scans [13]. These findings promoted high interest in understanding the dynamics of FC in health and disease, and thus, in the development of novel analytic approaches to study the variations in FC in the resting brain (discussed in [11]). Analysis of the resting-state FC course in patients with schizophrenia depicted a pronounced reduction in the number and diversity of connectivity states when compared to healthy individuals, reflecting alterations in brain communicational dynamics associated with schizophrenia [14].

FC measurements in schizophrenia are drawn primarily from fMRI scanning data, obtained from adults diagnosed with the disease. Since fMRI relies on hemodynamic fluctuations related to neural activity, it is not suitable for measuring brain activity with

high temporal resolution; thereby, it may miss fast transitions in brain FC configurations. Additionally, the spatial resolution of this technique is low. The typical size of fMRI voxels is around $3 \times 3 \times 3 \text{ mm}^3$, reflecting the average activity of hundreds to thousands of neurons [15]. Such volume covers the entire cortical thickness, containing several cell types with distinct morphological and functional properties. Thus, there is still a gap in our understanding of the cellular mechanisms involved in brain FC anomalies in schizophrenia.

Synapses are the elementary structural and functional units supporting information flow between individual neurons across the brain. Accordingly, the study of neuronal communication at the cellular level may increase our understanding of FC alterations observed in patients with schizophrenia. Human-induced pluripotent stem cells (hiPSCs)-derived models reflect the entire genetic component of patients with complex polygenic brain disorders [16], such as schizophrenia. These cells can faithfully recapitulate neurogenesis and the evolution of spontaneous network activity during brain development [17-22]; therefore, these cultures represent a novel strategy to obtain patient-derived neurons and study the underlying neuronal mechanisms of developmental psychiatric diseases. While so far it is not possible to reproduce the complexity of specific brain regions and their connectivity patterns, this *in-vitro* neuronal model could facilitate the exploration of general properties of FC dynamics in emerging neuronal networks. With this aim, we differentiated hiPSCs derived from patients with schizophrenia and healthy control donors into long-term neuronal cultures. Using Ca^{2+} imaging, we visualized local changes in fluorescence associated with spontaneous activity in large neuronal populations and measured the temporal correlation between signals arising from individual neurons. We adapted a FC analysis methodology, previously designed to study time-varying discrete connectivity states at whole brain level in schizophrenia [14], to quantify resting-state FC dynamics at the cellular level. As compared to the networks derived from healthy controls, neuronal networks derived from schizophrenia patients exhibited both a reduced ability to explore different functional connectivity configurations and a reduced competence for rapid connectivity reshaping, suggesting that alterations in neuronal communicational dynamics are already present during early development in schizophrenia and may contribute to the brain FC anomalies described in schizophrenia patients. These observations could have global implications for understanding the communicational

properties of the brain in patients with schizophrenia and may open new routes for exploring fundamental principles that rule brain communication through different spatiotemporal scales, in normal and pathological contexts.

Materials and methods

Description of the donors and cell lines

The hiPSCs lines used in this study were obtained from three healthy controls and four schizophrenia donors, all of whom displayed a normal karyotype. Detailed information about donors and samples is presented in Table S1. All the schizophrenia patients presented a high probability of a genetic predisposition to schizophrenia, based on the existence of relatives with the disease. Additionally, to decrease genetic heterogeneity among the cell lines, two of the donors are siblings. schizophrenia#1 is a male with paranoid schizophrenia, while his sister schizophrenia#2 was diagnosed with schizoaffective disorder and presented a history of drug abuse (cell lines are available at Coriell [23]). Schizophrenia#3 and schizophrenia#4 are males who were diagnosed with schizophrenia according to the DSM-IV Axis IV criteria, both exhibiting resistance to clozapine, with a family history of schizophrenia and no major psychiatric comorbidities, no history of head trauma and no drug or alcohol abuse. The cell lines from schizophrenia#3 and schizophrenia#4 were reprogrammed at D'Or Institute for Research and Education [24]. Considering the high likelihood of a genetic risk component to the disease within the patients' family members, the selected controls are not related to the patients. Healthy control#1 is a female and the cell line is available at Coriell. Healthy control#2 and healthy control#3 are both males and the cell lines were reprogrammed at the D'Or Institute for Research and Education. The establishment of hiPSCs and derivation of Neural Stem Cells (NSCs) was carried out according to the international standards and the approval of the Research Ethics Council "Comité de Ética em Pesquisa – Hospital Copa D'Or" (Certificado de Apresentação de Apreciação Ética (CAAE): 32385314.9.0000.5249).

Differentiation of NSCs to mature neuronal cultures

hiPSCs-derived NSCs were kindly donated by Dr. Stevens Rehen from the D'Or Institute and Federal University of Rio de Janeiro. Differentiation of hiPSCs to NSCs was performed as described in [25]. NSCs differentiation to mature neuronal networks was conducted by adapting the protocol of Shi et al. [26]. NSCs were thawed and seeded in Geltrex-coated plastic 60 mm plates and maintained in Neural Expansion Media (NEM; DMEM/F12 and Neurobasal medium (1:1) plus Neural Induction Supplement; Thermo Fisher Scientific, Carlsbad, CA, USA) until they reached 80-

100% confluence. Next, NSCs were detached from the plate with accutase (7 min/37°C), centrifugated at 300g for 4 min and resuspended in NEM plus 10 µM Rock Inhibitor (Y-27632; Merck, Darmstadt, Germany). 1×10^6 cells were plated in 35 mm petri dishes coated by poly-l-ornithine/laminin (10 µg/ml and 2.5 µg/ml, respectively). After 48 h, the medium was replaced by Neural Differentiation Media (NDM; DMEM/F12 and Neurobasal medium (1:1) supplemented with 1×N2, 1×B27 and 2-Mercaptoethanol 100µM). NDM was changed every two days. 14-16 days after plating, cells were detached with accutase and passed in a 1:3 ratio into 35 mm poly-l-ornithine/laminin-coated plates. Medium changes were done every 2 days. Around day 30, cells were passed into their final coated 35mm plate, in a 1:4 ratio (~ 500.000 cells per 35 mm petri dish). Cells were maintained in NDM, with medium changes every other day, for 60 more days.

Immunofluorescence

At 60 or 100 days of differentiation, cells were fixed with paraformaldehyde 4%, permeated with Triton-X (Sigma, St. Louis, MO, USA) 0.2%, blocked with BSA 5% in PBST (tween-20 0.1% in PBS), and incubated overnight at 4°C with anti-tau1 (mouse; #MAB3420 Millipore), anti-synaptophysin (mouse; #101011 Synaptic Systems), anti-MAP2 (rabbit; #AB5622 Millipore), anti-homer-1 (rabbit; #160002 Synaptic Systems), anti-GFAP (rabbit; #G9269 Sigma), and anti-TUJ1 (mouse; Sigma T8660). Subsequently, cells were incubated with secondary antibodies (goat anti-mouse Alexa 488, goat anti-rabbit Alexa 555, Invitrogen). Nuclei were stained with 4'-6-diamino-2-phenylindole (DAPI) 1µg/mL for 5 min. Images were acquired with a Zeiss LSM 710 confocal microscope.

Electrophysiology

Whole-cell voltage-clamp recordings were performed at 60 days of differentiation in control and schizophrenia derived cultures. Neurons were selected following morphological criteria. Na⁺ inward and K⁺ outward currents were evoked by voltage steps ranging from -100 to +40 mV in 10 mV increments ($V_{\text{hold}} = -75$ mV). Data were acquired at 50 kHz and low-pass filtered at 2.9 kHz, by an EPC-10 amplifier (HEKA Elektronik GmbH, Reutlingen, Germany). Patch electrodes (~4.5 MΩ) were pulled from borosilicate. The internal solution contained (in mM): 135 K-gluconate, 2 MgCl₂, 2 Na₂ATP, 0.3 NaGTP, 10 HEPES, 7 NaCl (pH 7.4). The recording chamber was

continuously perfused at 1–2 ml/min with ACSF solution containing (in mM): 115 NaCl, 2.5 KCl, 1.3 NaH₂PO₄, 26 NaHCO₃, 25 glucose, 5 Na-Pyruvate, 2 CaCl₂ and 1 MgCl₂ (300 mOsm/kg), gassed with 5% CO₂/95% O₂ (pH 7.4). Recordings were performed at room temperature (20–25 °C). Series resistance (10–40 MΩ) were not compensated and recordings were discarded for variations higher than 20% along the experiment.

qPCR

For qPCR analysis, we used neuronal cultures derived from three schizophrenia (#1,3,4) and three healthy control (#1-3) cell lines. Cellular cultures from early differentiated cells (30 days) and late differentiated cells (range of 70-91 days, herein defined as 90 days) were stored in Trizol (Thermo Fisher Scientific, Carlsbad, CA, USA) at -80°C. Samples obtained from the same cell line but from independent differentiation procedures were pooled together to extract total RNA. cDNA was synthesized from 1 µg RNA, using an M-MLV reverse-transcription kit (Promega, Madison, WI, USA). Primers were specifically designed to measure the expression of the genes listed in Figure S1A. Relative gene expression was assessed by qPCR (Agilent Technologies Thermocycler, Santa Clara, CA, USA). mRNA levels were calculated as the fold-change expression via $2^{-\Delta\Delta C_t}$ and gene expression was normalized to three different housekeeping genes (*B2M*, *18S*, *GAPDH*). Fold changes were assessed relative to a control sample (HC #1) or differentiation time.

Conditioned medium (CM) collection and neuro-proteomic profile

The presence of 30 different neuronal growth factors in serum-free collected CM (48 h) from cell cultures of 75 days of differentiation (four schizophrenia (#1-4) and three healthy controls (#1-3)), was evaluated using the Human Neuro Antibody Array II (#ab211063, Abcam, Cambridge, UK). Spots were detected by chemo-luminescence and intensity was quantified by densitometry (ImageJ, NIH, USA). The levels of each factor were measured in duplicates and normalized to internal controls provided by the assay.

Statistical analysis for mRNA expression and neuro-proteomic profile comparisons

mRNA fold-change normality was assessed with D'Agostino-Pearson and group comparison was done using a Nested t-test and linear mixed effect modelling, with a random intercept for cell line identity (id) (Table S2). Group comparison in terms of the

secreted proteins, measured with the neuro-proteome array, was also performed with linear mixed effect modelling. To evaluate the significance of the regression coefficients associated with the diagnosis (group), we used a Z test and Bonferroni correction for multiple comparisons. Statistical significance was set at $p < 0.05$.

Calcium imaging

Ca²⁺ transients were recorded from single cells across different regions of the plate showing high cellular density at 80-90 days of differentiation, using the cell-permeant Ca²⁺ indicator Oregon Green™ 488 BAPTA-1 (OGB-1 AM; peak absorption = 493 nm; Thermo Fisher Scientific, Carlsbad, CA, USA). Epifluorescence imaging was performed with a mercury arc lamp and using a band pass excitation (450–490 nm) filter. Emitted light was detected with an electron-multiplying CCD camera (High Performance CCD Sencicam, PCO Cooke) with a band pass filter (515-565). Three schizophrenia (#2, 3, and 4) and two healthy control (#1 and 2) cell lines were analyzed (2-3 plates per cell line; 3-27 neuronal aggregates per plate). The loading solution consisted of OGB1 3.2 μ M, Cremophor EL (Merck, Darmstadt, Germany) 0.01% v/v and Pluronic F-127 (Merck, Darmstadt, Germany) 0.4% in NDM. Cells in the loading solution were incubated for 1 hour in the dark at 37°C and 7% CO₂. After washing twice with NDM, the medium was replaced with ACSF, and cells were maintained for 30 min before imaging. The regions of interest were recorded for ~ 4.7 min at 6.64 Hz (T = 0.1506 s; 1877 frames in total). TTX (0.2 μ M) was added to the bath to confirm the AP-dependence of Ca²⁺ transients.

Imaging analysis

Data pre-processing

Bleach correction was conducted for all recordings with the ImageJ Bleach Correction Macro Package [27]. Contrast and brightness were adjusted manually using ImageJ tools. Motion correction and active neurons identification were performed with the CalmAn Constrained Nonnegative Matrix Factorization algorithm [28]. We will use the term “network” to refer to all the identified active neurons by CalmAn within the recorded visual field. Therefore, within each plate, several networks were recorded. Ca²⁺ transients (Figure 2C-D) in every active neuron were obtained by subtracting the neuron baseline fluorescence (quantile 8), and a fluorescence intensity matrix was built

per network with rows corresponding to the different neurons and columns indicating the Ca^{2+} signal at every frame (point in time) during the recording time.

Network topology analysis

The Pearson's correlation index between the signals of every pair of neurons in each network (rows in the fluorescence intensity matrix) was calculated. A FC matrix (with shape: neuron identity, neuron identity) was created with these correlations (Figure 2E). Two neurons were considered as connected if the absolute value of the correlation index was > 0.4 (Figure 2F).

Frequency distribution of neuronal connectivity degree

For the Poisson and the Binomial fitting of the number of functional connections per neuron (connectivity degree; Figure 2G), we first built a histogram with binned connectivity degree data (11 bins). Then, the fitting was performed on the binned data with nonlinear least-squares regression using the *curve_fit()* function of SciPy python library, with *poisson.pmf()* for Poisson and *binom.pmf()* for Binomial fitting. For the power-law fitting (Figure 2H), the slope (scaling exponent) in each network was estimated by linearly regressing the logarithm (\log_{10}) of neurons connectivity degree on the logarithm of its frequency. The code employed to obtain the scaling exponents of each network is available at

https://github.com/sofiapuvogelvittini/neuronal_functional_connectivity. Then, a linear mixed effect model, adjusting for the number of neurons and number of possible connections in the network (described in Eq. 1), was used to compare the scaling exponents between schizophrenia and healthy controls.

Identification of individual calcium transient events

Individual events were detected using TaroTools extensions implemented in Igor Pro (Wavemetrics, Lake Oswego, OR, USA). After a first automatic round using an amplitude threshold-based detection of 40% of the maximum amplitude for each trace, we visually confirmed the selection of events before subsequent analysis. The half-width was measured in 5,246 detected events and a histogram was built to visualize the distribution of individual events kinetics (Figure 3A.I)

Functional connectivity dynamics

To identify the different connectivity configurations occurring in the network during the recording period, we applied a sliding-time-window correlation method to the fluorescence intensity matrix [11]. This consists in calculating the Pearson's correlation index for the signals of every pair of neurons in the network within a defined number of frames (width of the time-window). The window is then shifted in one step, to frame $t+1$, repeating the procedure until all frames are covered (Figure 3A.II). Thereby, a FC matrix is obtained per step ($wFC(t)$; Figure 3B.I). After measuring the kinetics of all detected calcium transients (see half-width histogram of Figure 3 A.I), we chose a width for the time-window of 70 frames (~ 10.5 s), to capture the vast majority of different connectivity configurations while minimizing random correlations within the signal noise. To assess the sensitivity of our framework to changes in this parameter, we repeated the procedure using longer time-windows of 100 and 200 frames. As the $wFC(t)$ matrices are symmetrical, we reshaped them into a one-dimensional vector containing only the values below the diagonal. FC dynamics matrices (FCD) were then obtained by computing the Pearson's correlation coefficient between every pair of $wFC(t)$ vectors (Figure 3B.II).

Functional connectivity meta-states

To quantify and compare the dynamics of FC in our networks, we adjusted a method designed by Miller et al (2016) [14] for fMRI data that allows both identification of discrete connectivity configurations and extraction of relevant features of FC dynamics. For each network, we conducted an independent component analysis (ICA) along the whole set of $wFC(t)$ vectors, using the FastICA algorithm [29]. Setting the same number of independent components across all the networks, we reduced the dimensions of all $wFC(t)$ to a same number. The number of independent components was set to four, allowing algorithmic convergence in most recordings. Each $wFC(t)$ vector was regressed on the four independent components or "correlation patterns" (CP; note that each network had its own specific CP basis) and the original vector was then described by the four corresponding regression coefficients or "weights", each one associated with a CP (Figure 3B.III). Next, the weights were discretized into quartiles (Figure 3B.IV). As weights could be positive or negative, we treated them separately during the discretization process. We replaced CP weights by a value in $\pm (1,2,3,4)$, according to their signed quartile. A meta-state was then defined by a particular combination of

four discretized weights and, while all networks presented the same number of potential meta-states, each network would typically visit a subset of them.

Functional connectivity-related variables

After obtaining the set of visited FC meta-states per network, we calculated the following FC-related variables describing the dynamics of the network connectivity:

- Number of visited meta-states: total number of different meta-states realized by each network.
- Number of change-points: number of transitions through the visited meta-states.
- Meantime in a meta-state: mean number of consecutive frames that the network remained in a meta-state, translated to units of time.
- Maximum distance between successive meta-states: maximum Manhattan distance (L1) between two consecutive meta-states.
- Traveled distance: sum of the distances between successively visited meta-states along the entire recording time.
- Dynamic range: Manhattan distance (L1) between the most distant visited meta-states.
- Number of hub meta-states: total number of different meta-states visited at least twice during the recording time.
- Meantime in a hub: mean number of consecutive frames that the network remained in the same hub meta-state, converted to units of time.
- The number of visits to hub states: number of times that the network visited any hub meta-state.

The number of frames was translated to units of time by multiplying it by the camera delay (~ 0.1506 ms). Identification of meta-states and quantification of FC-related variables were performed using customized code written in Python, which can be found at https://github.com/sofiapuvogelvittini/neuronal_functional_connectivity. Since the FC-related variables were quantified in each different network, multiple measurements were obtained per cell line. Therefore, the “schizophrenia effect” (diagnosis effect) was evaluated with a mixed linear regression model, including a random intercept for the cell line identity (id) to account for the internal variability within the different cell lines. As in most cases the FC-related variables correlated with the number of active neurons (see Results, Figure S5B), we used deviance statistics to evaluate the necessity to

adjust for the number of neurons and number of possible connections. In such cases, the variables were previously centered.

We used the Statsmodels package of Python to fit the following model:

$$y \sim \beta_{diagnosis} X_{diagnosis} + \beta_{(\#ofneurons)} X_{(\#ofneurons)} + \beta_{(\#ofneurons)^2} X_{(\#ofneurons)^2} + (1|cell\ line\ id)$$

(Eq. 1)

y represents the dependent variable and can take the value of any FC-related variable, as well as the value of the scaling exponents obtained from the connectivity degree power-law fitting. β_i are the coefficients associated with the X_i predictors. $X_{diagnosis}$ is a binary variable, coded as “1” for schizophrenia neurons and as “0” for healthy controls. Thus, the “schizophrenia effect” corresponds to the value of $\beta_{diagnosis}$ and was considered statistically significant when its Z-score-associated p value was < 0.05 . $\beta_{diagnosis} > 0$ indicates a positive correlation of the variable y with the schizophrenia condition, and the opposite for $\beta_{diagnosis} < 0$.

More details and specifications of the regression models are presented in Supplementary tables 3-5.

Results

Molecular profiling of long-term hiPSCs-derived neuronal cultures from schizophrenia and healthy controls

Given the relative scarcity of studies on functional maturation in long-term hiPSCs-derived neuronal cultures, we first aimed to validate and characterize the differentiation process. We used hiPSCs-derived NSCs cultures from healthy controls and schizophrenia patients, displaying clear staining for NESTIN and PAX6, two well-known markers for NSCs [25]. We modified the protocol of Shi et al., 2012 [26] to induce long-term neuron-enriched cell cultures from four schizophrenia and three healthy control NSCs lines (see Table S1 for details). We omitted the use of antibiotics, as they may affect neuronal excitability [30] and modify the expression of several genes [31]. Healthy control and schizophrenia patient-derived NSCs aggregated and formed neuronal rosettes that became larger and defined along the differentiation process [21]. After 30 days, 3D neuronal aggregates were already easily identified (Figure 1A-D), exhibiting unique structures that vary in size and shape within each culture plate. At 60 days, neurons expressed specific dendritic and axonal markers (MAP2 and TAU, respectively); MAP2 was expressed in the perikarya and dendrites (Figure 1E, G), while TAU was mainly expressed in axons (Figure 1F, H). Also, the expression of the pan-presynaptic vesicle-associated protein synaptophysin (SYP; Figure 1E, G) and the postsynaptic scaffolding protein (HOMER1) (Figure 1F, H) confirmed the presence of synaptic structures. In addition, hiPSCs-derived neurons from both healthy controls and schizophrenia displayed voltage-dependent Na⁺ and K⁺ currents (Figure 1I, J). Consistent with Shi et al., 2012 [26], at 100 days of differentiation we observed the presence of GFAP⁺ astrocytes, mostly in the surrounding area of the neuronal aggregates (Figure S2).

The functional competence of our differentiated cell cultures was further assessed by analyzing their conditioned medium (CM). The expression profile of different cytokines and growth factors related to neuronal differentiation and signaling was evaluated in the serum-free CM, collected from schizophrenia and healthy control cell lines (Figure 1K) at 75 days of differentiation. The complete set of targeted proteins was identified in the CM (although Eotaxin-3 and Interleukin-18 were barely detected; Figure S3) of schizophrenia and control neurons, and quantification of the secreted proteins revealed a similar secretion profile between the two groups. Altogether, these results

validate the correct establishment of healthy control and schizophrenia mature neuronal cultures.

Altered expression of genes involved in synaptic function and network establishment during schizophrenia neurodevelopment

We analyzed the expression of a set of genes involved in synaptic function, cytoskeleton organization, and cellular metabolism in our neuronal cultures. Gene expression was quantified with qPCR at two different time points during the differentiation process: 30 and 90 days in culture (Figure S1A and S1B). We evaluated genes encoding selected proteins expressed in glutamatergic synapses, including the glutamatergic NMDA-receptor subunit 1 (*GRIN1*) and *HOMER1* [32]; as well as genes encoding GABAergic synapse markers, such as the GABAergic postsynaptic anchoring protein (*GEPHYRIN*), associated with GABA receptors [33], and the glutamic acid decarboxylase 67 (*GAD67*), involved in the synthesis of GABA [34]. Also, we quantified the expression of *SYP*. Schizophrenia and healthy control neurons did not display significant disparities in the expression of the mentioned genes when compared at the same period of differentiation (Figure S1B). To explore how potential glutamatergic and GABAergic synapses evolved over time in both conditions, we quantified the change in mRNA expression of the mentioned genes between 30 and 90 days *in-vitro* (90/30 days ratio; Figure 1L-P; for details on statistical tests and *p* values, see Materials and Methods and Table S2) and compared this change between schizophrenia and healthy control networks. The change in *HOMER1* expression along differentiation was significantly different between both conditions (Figure 1L); while its expression decreased in healthy controls, it increased in schizophrenia (Table S2). A difference between groups was also detected for *GRIN1*, with a significant decrease of *GRIN1* expression activity during differentiation in healthy controls and no change in schizophrenia (Figure 1M, Table S2). These results suggest a divergent evolution in the number, or strength, of excitatory synapses during early neurodevelopment in schizophrenia, as compared to healthy control networks. On the other hand, expression of the GABAergic marker *GPHN* was reduced in both conditions along this period of time (Table S2), suggesting a decline in GABAergic communication during differentiation, and no difference was observed in *GPHN* expression change during the assessed period between schizophrenia and healthy control neurons (Figure 1N). Also, no difference in *GAD67* expression change during differentiation was observed

in schizophrenia as compared to healthy control networks (Figure 1O). Conversely, the expression of *SYP* remained unaltered in healthy control neurons during the evaluated time period, whereas it increased in schizophrenia networks (Figure 1P). Considering the increase in *HOMER1* and *GRIN1* expression in schizophrenia networks during the differentiation process, the increase in *SYP* might reflect an increased number/activity of excitatory synapses in schizophrenia, further supporting an altered evolution of synaptic connectivity over time in schizophrenia. In this same line of evidence, a recent work using immunofluorescence staining indicated a higher density of SYP puncta in hiPSCs-derived neurons from patients with schizophrenia [35]. Altogether, these observations support previous hypotheses proposing an altered excitatory/inhibitory balance in schizophrenia [36], with a trend to develop hyper-excitability, and suggest that this imbalance may have its origin in the early stages of neurodevelopment.

We also evaluated expression changes during differentiation of *CDK5R1* and *RELN*, both involved in neurodevelopment. *CDK5R1* codes for p35, the neuronal-specific activator of cyclin-dependent kinase 5 (CDK5) regulatory subunit 1 [37]. CDK5 contributes orienting neuronal network structure during neurodevelopment via cytoskeleton remodeling [38]. Expression of p35, and hence CDK5 activity, varies cyclically along with brain development [39]. During the assessed period, we found a reduction in *CDK5R1* expression in both conditions (Table S2). Nonetheless, this decrement was significantly lower in schizophrenia than in healthy control cultures (Figure 1Q).

The extracellular-matrix glycoprotein RELN plays a critical role in neuronal migration during early development [40]. Later in life, it modulates dendritic and axonal outgrowth and spine maturation, by regulating cytoskeleton dynamics. In our neuronal cultures, the change in *RELN* expression between the 30 and 90 day of differentiation was similar for schizophrenia and healthy controls (Figure 1R).

Since metabolic anomalies were associated with schizophrenia [41], we also evaluated the expression of *ATP5*, coding for mitochondrial-membrane ATP synthase. *ATP5* expression decreased throughout the evaluated period in healthy control networks, but remained unchanged in schizophrenia (Figure 1S, Table S2). An abnormal energy metabolism during early neurodevelopment might have multiple consequences on network establishment and function [42].

Finally, we did not detect changes in gene expression level of glucose transporter 1 (*GLUT1*), nor in the expression of the semaphorin family *SEMA3A*, along differentiation (Table S2, Figure 1T-U).

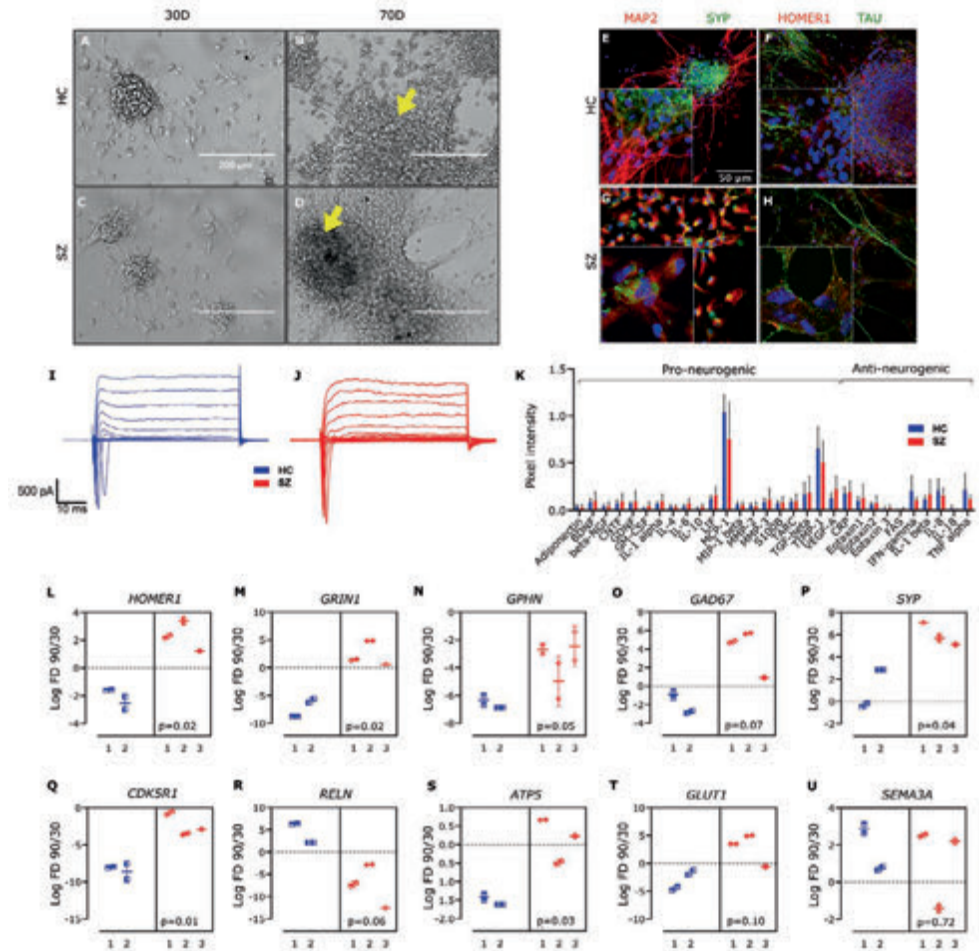


Figure 1. Profiling of hiPSCs-derived neurons obtained from healthy controls and schizophrenia patients.

(A-D) Representative images for healthy control- (A, B) and schizophrenia- (C, D) derived neuronal cultures, captured with phase-contrast microscopy at 30 (A, C) and 90 (B, D) days of differentiation. Arrows indicate 3D neuronal aggregates where spontaneous activity was recorded. Calibration bar: 200 μ m. (E-H) Representative immune staining for the dendritic and axonal markers MAP2 (E, G) and TAU (F, H), respectively, as well as for the pan-presynaptic and glutamatergic-postsynaptic proteins synaptophysin (SYP) (E, G) and HOMER1 (F, H), respectively. DAPI staining is shown in blue. Calibration bar: 36 μ m. (I, J) Representative voltage-clamp electrophysiological recordings at 60 days of differentiation, for healthy control and

schizophrenia-derived neurons. **(K)** Quantification of neurogenic protein levels (mean \pm SD) in the CM of four schizophrenia (#1-4) and three healthy control (#1-3) cell lines at 75 days of differentiation. **(L-U)** Fold-change in mRNA expression levels of different genes related to central nervous system development, in the period from 30 to 90 days. Data is presented as the log₂ of the 90/30 days ratio for three schizophrenia (#1, 2, and 3) and two healthy control (#2 and 3) cell lines, and every observation is reported independently. *B2M* was used as housekeeping. Excepting *SYP* in SZ#1, all measurements were performed in duplicates per cell line; *p* value (*p*), from nested t-test. Schizophrenia (SZ), Healthy control (HC).

Calcium imaging in hiPSCs-derived neuronal networks

Spontaneous spiking activity of hiPSCs-derived populations of neurons was registered at single cell resolution, by monitoring changes in intracellular Ca²⁺ concentration [43]. Cell cultures were loaded with the cell-permeant version of the Ca²⁺ indicator OGB1 (Figure 2A, 2B) and 4.7 min length videos (1,877 frames per video; T = 0.1506 s) were recorded across different regions of interest (ROIs) within the cell plates. As previously described [21], higher neuronal density and spontaneous activity was more likely to be found in cell aggregates protruding from the base of the plate (Figure S4 and yellow arrows in Figure 1B, D). Therefore, we considered them as the ROIs to study local neuronal network activity. We identified the active neurons within these ROIs using the open-source tool CalmAn software, considering a signal-to-noise ratio above 2.5 [28], and the set of active neurons in the aggregate was defined as a neuronal network (134 networks in total, 3-27 networks per plate, 2-3 plates per cell line, 3 schizophrenia and 2 healthy control cell lines). Then, Ca²⁺ transients were obtained from every neuron in the network (Figure 2C and 2D). The number of active neurons within each network varied from 15 to 250; however, regression analysis revealed no difference in the mean number of active neurons per network between schizophrenia and healthy controls (Figure S5A, mixed regression model detailed in Materials and Methods Eq. 1).

Voltage-gated Na⁺ channels are responsible for the initiation and propagation of action potentials in neurons [44]. To probe the action-potential dependency of the spontaneous Ca²⁺ events observed in the networks, we added the selective Na⁺ channel blocker toxin tetrodotoxin (TTX; 0.2 μ M) to the bath during recordings. Ca²⁺ transients were abolished by the blockage of the voltage-gated Na⁺ channels (Figure S6), corroborating the neuronal origin of the detected activity.

Network topology analysis of hiPSCs-derived neuronal cultures based on functional connectivity measurements

Previous studies assessed neuronal structural connectivity in hiPSCs-derived neurons using trans-neuronal spread of rabies virus [19, 45]. Neuronal cultures derived from schizophrenia patients presented a decrease in trans-synaptic tracing [45], which might be related to a decrement in the number of synaptic connections. However, contrary to this hypothesis, electrophysiological recordings indicated similar total spontaneous synaptic activity between schizophrenia and healthy control neuronal cultures [45]. In the present work, we addressed neuronal network connectivity from a functional perspective by quantifying the co-variation in neurons activity patterns, registered with Ca^{2+} imaging, in schizophrenia and healthy controls. Since the underlying network topology frames neuronal interactions, assessing FC in this *in-vitro* system represents both an indirect approach for revealing the structure of the networks and a direct way to interrogate their emerging functional properties.

To quantify neurons FC, we calculated the Pearson's correlation index for the Ca^{2+} signals from each pair of neurons in every network. As a first approach, we considered the entire recording time (4.7 min) and generated a FC matrix (or correlation matrix) displaying the correlation indexes between each pair of neurons (Figure 2E). Then, the number of functional connections per neuron was obtained from this FC matrix, by considering a pair of neurons as functionally connected when the correlation index was above 0.4 or below -0.4. For an absolute correlation value of 0.4 as a cut-off point, the pairs of functionally connected neurons reached 25% of the total possible connections, considering all networks (Figure 2F). If the total number of connections per neuron was randomly determined, the probability for a neuron to have "x" connections (connectivity degree) would follow a binomial distribution, and for large enough populations, a Poisson distribution (Figure 2G). In contrast, the probability distribution for the number of connections per neuron was right-skewed, resembling a 'scale-free' distribution (Figure 2H; also known as 'long-tailed' or 'power-law' distribution). This suggests that a large number of neurons had few active connections, while a small number were hyper-connected (Figure 2G, H, I). Interestingly, this connectivity organization has been proposed for the CNS across different species, including humans [46, 47], and our results add evidence suggesting that it might be conserved in early neurodevelopment.

The scale-free fitting of neurons connectivity degree followed a power-law with a scaling exponent of -1.4 (Figure 2H). Using trans-neuronal spread of rabies virus, a previous analysis of network topology in hiPSCs-derived neurons demonstrated that the number of structural connections of the neurons also followed a scale-free distribution, with power -2 [19]. Taken together, these observations support the suitability to explore topological properties of hiPSCs-derived neuronal networks through FC analysis, by establishing a link between structural and functional communication.

To test for differences in the functional topology between schizophrenia and healthy controls, we fitted a mixed linear model for the networks power-law scaling exponents, including a varying random intercept for cell line id and adjusting for the number of neurons and number of total possible connections in each network (see Methods Eq. 1). The functional topology of schizophrenia networks did not deviate significantly from the healthy control networks topology (Figure 2I).

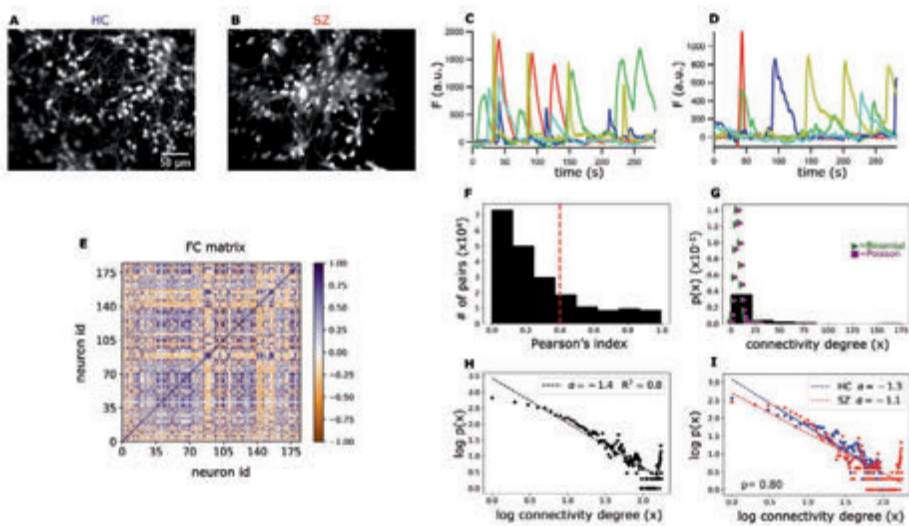


Figure 2. Functional connectivity (FC) and topology analysis in healthy control and schizophrenia networks.

(A, B) Representative ROI images of healthy control and schizophrenia neuronal cultures loaded with the Ca^{2+} indicator OGB-1. (C, D) Ca^{2+} transients (fluorescence intensity after baseline correction) of 5 randomly selected neurons in a healthy control and a schizophrenia network. (E) Representative static FC matrix displaying the Pearson's correlation indexes (color bar) between the Ca^{2+} signals from each pair of neurons in a healthy control network, considering the whole recording time. (F)

Frequency plot of the absolute Pearson's correlation coefficients from every pair of neurons, considering all networks. The dotted red line indicates the threshold beyond which we considered a pair of neurons as functionally connected. **(G)** Probability density of finding a neuron with x functional connections (connectivity degree). The connectivity distribution does not fit to a Poisson ($\lambda = 8$) nor to a Binomial ($n = 1000$, $p = 0.008$) distribution. **(H)** Scatter plot of the connectivity degree logarithm (\log_{10}) versus the probability logarithm. Data fit a scale-free or long-tailed distribution, with a scaling exponent of -1.4 . **(I)** Scale-free fitting of neurons connectivity degree in schizophrenia and healthy control networks. Connectivity scaling exponents were fitted with a mixed effect regression model detailed in Materials and Methods. The scaling exponents did not significantly differ between the two groups. P value (p). Schizophrenia (SZ), Healthy control (HC).

Functional connectivity in hiPSCs-derived neuronal networks is dynamic and goes through reoccurring configurations

The FC analysis of resting networks described so far represents the average connectivity among pairs of neurons along the entire recorded time (4.7 min). However, this approach does not allow to explore dynamic fluctuations of connectivity that could occur within shorter periods of time.

The temporal dimension of the FC in the hiPSCs-derived networks was addressed with a sliding-time-window correlation method [11] (Figure 3A). To choose an appropriate width for the time-window, we first built a histogram depicting the distribution of the half-width of all detected Ca^{2+} events ($n = 5,246$; Figure 3A.I). As no events with a half-width longer than 10 s were detected, we used a sliding time window of width = 10.5 s (70 frames, Figure 3A.II) to capture most of the different connectivity configurations while minimizing random correlations within the signal noise. For each network, we obtained a set of windowed FC matrices ($wFC(t)$; where t is the time step, running from 1 to 1,808) (Figure 3B.I). Then, we computed the correlation matrix for every pair of $wFC(t)$, obtaining a time versus time functional connectivity dynamics matrix (FCD) (Figure 3B.II). The FCD diagonal results from comparing the same time points, thus displaying full correlation. Points located adjacent to the diagonal (Figure 3B.II, black dotted squares) are also expected to present high correlation, since they correspond to nearby, partially overlapping, time-windows. However, the squared blocks far away from the diagonal (Figure 3B.II, red dotted squares) suggest the reappearance of previously visited FC configurations in a distant time point. This reveals that, during the recording time, the network resting-state FC went through numerous and reoccurring

configurations, rather than evolving in an arbitrary way. Remarkably, this observation resembles previously described FC dynamics in the human brain at rest [13].

Next, we developed a quantitative framework to evaluate and compare the dynamics of FC between schizophrenia and control networks, by modifying a previously published method that was designed to evaluate whole-brain functional connectivity dynamics in patients with schizophrenia [14]. To reduce the dimensions of the wFC(t) matrices, obtained from the different networks, to the same number of dimensions (note that the dimensions of the wFC matrices depend on the number of active neurons in the particular network), we ran an independent component analysis (ICA) [29] per network, throughout the temporal dimension of its FC (Figure 3B.I, tICA on the set of wFC(t)). This computational method allows the separation of a complex signal into additive components [29]. Four different and independent FC configurations, defined here as *correlation patterns* (CP), were identified per network. To describe each of the wFC(t) in terms of these four CP, we obtained four coefficients or “weights” by linearly regressing every wFC(t) on the CPs (Figure 3B.III). Then, to capture a finite number of FC configurations and to define the same maximum number of different FC states across all the networks, the weights were discretized into quartiles, allowing similar connectivity configurations to be grouped together (Fig 3B. IV). The unique combination of four discretized weights defined a Meta-state (MS), borrowing the term coined by Dr. Robyn Miller [14].

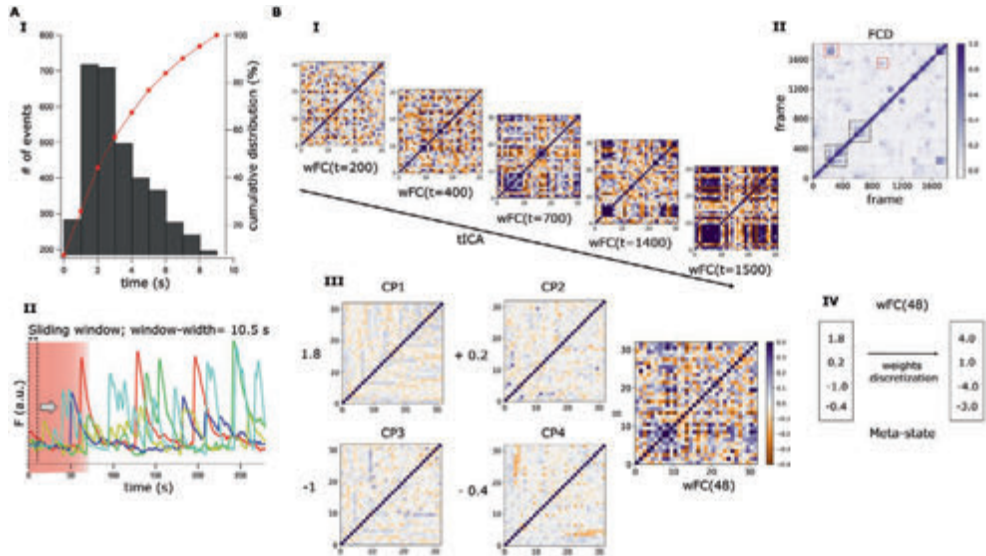


Figure 3. Dynamics of the resting-state FC and definition of connectivity Meta-states.

(A) Graphical representation of the sliding time-window correlation method. (A.I) Histogram showing the distribution of the transients half-widths for all detected Ca²⁺ events ($n=5,246$). The cumulative distribution (red curve) depicts that no event with a half-width longer than 10s was detected. (A.II) Ca²⁺ signals of 5 randomly selected neurons in a healthy control network composed of 32 active neurons. A sliding time-window of width 10.5 s (70 frames) is represented by a pink rectangle, within which the correlation between the signals originating from each pair of neurons is calculated. The time-window scrolls through the entire recording time (1,877 frames), advancing one frame at each step, and a windowed correlation matrix (wFC) of shape number of neurons, number of neurons, is obtained at each step (t). **(B)** Windowed correlation matrices and definition of Meta-states. (B.I) A wFC(t) is obtained for each time step (t), with t running from 1 to 1,808. (B.II) A representative Functional Connectivity Dynamics matrix (FCD) obtained from a healthy control network. This time versus time FCD matrix is obtained by calculating the Pearson's coefficient between every pair of wFC(t) in the network. Periods of lasting FC patterns are reflected by square blocks around the FCD diagonal (black dotted squares) and reoccurring patterns by square blocks distant from the diagonal (red dotted squares). (B.III) For every recorded network, an independent component analysis (tICA) is performed along the temporal axis of the whole set of wFC(t), and four independent connectivity patterns (CP) are obtained. Then, each wFC(t) can be described as a linear combination of these four CP and (B.III) shows wFC(48) as an example. The coefficients (weights) multiplying each CP are obtained by linearly regressing wFC(48) on the CPs. (B.IV) To have a finite number of states (meta-states, MSs), the weights associated with the CPs are discretized and assigned to their respective quartile. The combination of these four discretized coefficients describes a MS. Schizophrenia (SZ), Healthy control (HC).

Resting-state functional connectivity in schizophrenia networks is less flexible and slower in rearranging different configurations compared to healthy controls

By studying neuronal functional relationships in our *in-vitro* model, we aimed to test whether some features of the resting-state FC dynamics observed in schizophrenia patients [14] might also be observed in neural networks resembling early neurodevelopmental stages in schizophrenia. Using the methodology described in Figure 3, we obtained the FC MSs visited by each network and quantified a set of FC-related variables (listed and defined in Materials and Methods) in both conditions. Figure 4 aims to clarify the meaning of these variables, with Figure 4A illustrating examples of different possible MSs visited by a network and Figure 4B including a graphical explanation of the measured variables.

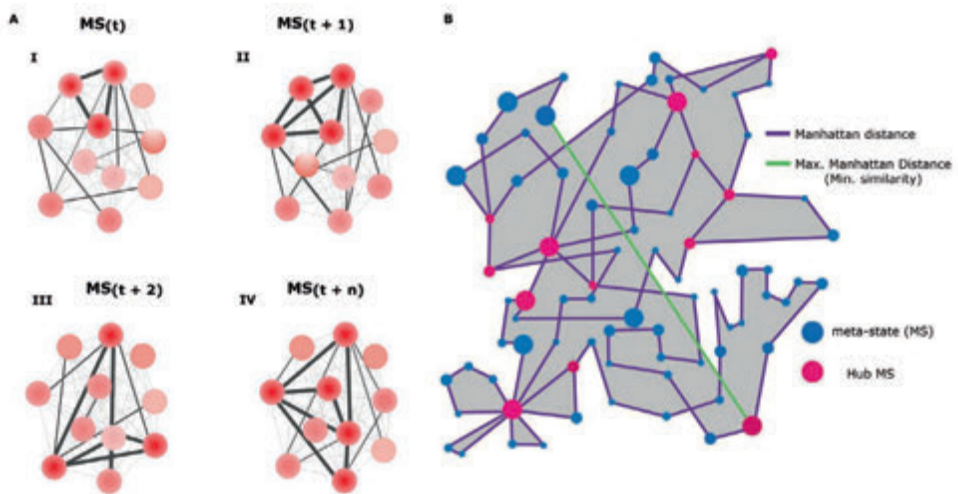


Figure 4. Functional connectivity-related variables.

(A) Schematics represent four possible functional connectivity meta-states (MSs), corresponding to particular activity configurations of the neurons conforming the network. Each circle represents a neuron and color intensity the strength of its activity (low red = low activity, high red = high activity). The thickness of the straight lines connecting the neurons reflects the strength of the correlation between the signals emitted by the neurons (thicker = higher correlation). **(B)** Diagram illustrating an example of the resting-state FC flow of a network, with a description of all measured FC-related variables. Blue circles represent the different visited MSs. Each MS inhabits a 4-dimensional space, determined by the 4 weights associated with the independent connectivity patterns. However, for visualization purposes, in this scheme each MS is represented in a 2-dimensional space with arbitrary units. Circle size denotes the

uninterrupted time (dwell time) spent by the network in each configuration. Purple lines represent successive transitions between different MSs. The length of the lines corresponds to the Manhattan distance between two connected MSs (in the space where the MSs reside) and reflects how different are successive MSs, with longer lines indicating higher dissimilarity. As a measure of network flexibility, we evaluated the ability of schizophrenia and healthy control networks to switch in just one step between two configurations that are as different as possible, a transition represented by the maximum distance achieved between two successive MSs (green line). The pink circles represent recurring MSs (Hub MSs), which are connected by more than two lines, meaning that the network visited them at least two times. The grey area corresponds to the dynamic range, a global indicator of the potential diversity of accessible MSs. The length of the trajectory of the purple line corresponds to the total traveled distance. Panels (A) and (B) were not generated from real data and constitute solely graphical illustrations.

Differences in FC-related variables between schizophrenia and healthy control networks were assessed using mixed linear regression modeling. Even though the average number of active neurons did not differ between schizophrenia and healthy control networks (Figure S5A), in most cases the measured FC-related variables correlated with it (Figure S5B). Therefore, we included the number of active neurons as a covariable in almost all the multiple regressions (Table S3).

We observed a reduction in the number of different MSs visited by schizophrenia networks (Figure 5A), suggesting a more limited repertoire of accessible configurations in schizophrenia, as compared to healthy control networks. We also measured the number of times that networks changed from one MS to another (Figure 5B), and the mean uninterrupted time spent in an MS (Figure 5C). Schizophrenia networks switched fewer times from one MS to another and remained longer at the same MS, evidencing a reduced dynamism. In addition, healthy control networks were capable to transit to more different (distant) configurations in one step (maximum distance between successive MSs, Figure 5D) than schizophrenia networks, suggesting that schizophrenia networks have less potential to fast switching between distant FC configurations, reflecting reduced flexibility. We also calculated the total traveled distance within the MSs inhabited space, defined as the sum of the distances between successive MSs through the whole recorded time (Figure 5E), finding that it was reduced in schizophrenia (Figure 5F). Finally, we evaluated the dynamic range by calculating the Manhattan distance between the farthest MSs visited along the whole trajectory, which is formally a measure of the size of the space containing the different

visited MSs (Figure 5G). We must bear in mind that the dynamic range is relative to the specific CPs of each network. Therefore, this measurement reflects how much the space where the different MSs inhabit is exploited with respect to the network intrinsic “motion possibilities” and can be interpreted as the potential of the network to flow through diverse connectivity configurations. We observed a reduced FC dynamic range in schizophrenia networks compared to healthy controls (Figure 5G), which is consistent with the lower number of different visited MSs and the reduced total traveled distance in schizophrenia networks, since a lower dynamic range would imply a decrease in FC motion potential.

Considering that the value of the FC-related variables might be sensitive to the width of the time-window, used to capture the visited MSs, we repeated the complete procedure for obtaining the MSs using two different time-windows of widths 100 and 200 frames (15.1 and 30.1 s, respectively), and compared the estimated FC-related variables between schizophrenia and healthy controls. The results of these analyses are depicted in Table S4 and S5. All the results were replicated for larger time-window widths (Table S4 and S5).

Summarizing, our observations suggest that resting-state schizophrenia networks have fewer available FC configurations, explore them less thoroughly and reorganize their activity patterns less rapidly as compared to healthy control networks. Overall, these findings point to a reduction in FC dynamism and flexibility in schizophrenia networks, involving speed and exploration potential.

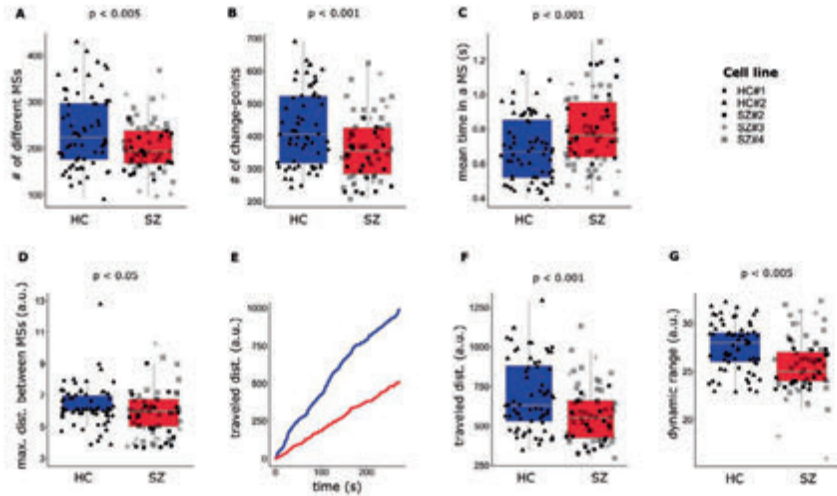


Figure 5. FC in schizophrenia networks is less dynamic than in healthy controls. (A) Schizophrenia networks visit a lower number of different meta-states (MSs) and (B) change fewer times from one MS to another during the recorded time, spending longer uninterrupted time at the same MS (C). (D) The maximum distance, Manhattan distance (L1), between successive MSs is reduced in schizophrenia neuronal networks. (E) A graphical representation of how FC travels within the space inhabited by the MSs, in terms of the L1 distance between successive visited MSs. The plot indicates the cumulative traveled distance, measured as the total traveled distance at each time point. (F) The overall distance traveled through the MSs space, calculated as the sum of all L1 distances across the visited MSs, is reduced in schizophrenia networks. (G) The intrinsic dynamic range, measured as the L1 distance between the most distant MSs, is also reduced in schizophrenia networks. Each single data is plotted independently on the boxplots and its symbol indicates the cell line of the particular network. For each dependent variable (Y-axis), the p value (p) associated with the effect of the diagnosis from the regression model (Table S3) is indicated. A time-window of width = 70 frames (~ 10.5 s) was used for capturing the visited MSs. Schizophrenia (SZ), Healthy control (HC).

Schizophrenia networks display a reduced number of recurrent functional connectivity meta-states (hub MSs) as compared to healthy control networks

As mentioned before, neuronal networks went through different FC configurations that reoccurred during the acquisition time (Figure 3B.II, FCD matrix). Therefore, we quantified the number of different MSs that were revisited by each neuronal network. In whole brain fMRI FC analysis, these recurrent MSs have been named as “hub meta-states” [14], and here we named them in the same way. Schizophrenia networks

displayed a lower number of different hub MSs (Figure 6A) and visited these hub MSs less often than healthy control networks (Figure 6B), but spent longer uninterrupted time in them (Figure 6C). These results were replicated when a larger time-window width of 100 frames (15.06 s) was used for obtaining the visited MSs (Table S4). However, the differences between schizophrenia and healthy control networks in terms of the number of different visited hub MSs and the number of visits to hub MSs were no longer observed for a time-window width of 200 frames (Table S5).

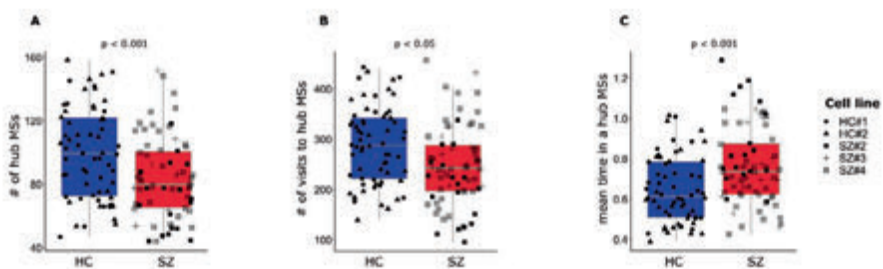


Figure 6. Schizophrenia networks visit a lower number of different hub MSs but remain longer uninterrupted time in them.

(A) The number of different visited hub MSs is lower in schizophrenia networks. **(B)** Schizophrenia networks visit hub MSs less often than healthy control networks, but **(C)** spend longer uninterrupted time in the same hub MS. Each single data is plotted independently on the boxplots and its symbol indicates the cell line of the particular network. For each dependent variable (Y-axis), the p value (p) associated with the schizophrenia effect from the regression model (Table S3) is indicated. A time-window of width = 70 frames (~ 10.5 s) was used for capturing the visited hub MSs. Schizophrenia (SZ), Healthy control (HC).

Discussion

Cognitive functions require the integration of neural activity through different scales, from neurons and local circuits to large-scale brain networks. Considering the evidence pointing to FC alterations in patients with schizophrenia [5-8, 14], this study aimed to evaluate whether FC differences between schizophrenia patients and healthy control subjects could be explored during early nervous system development *in-vitro*, using hiPSCs-derived neuronal networks. Our data indicate that FC in schizophrenia neuronal networks is characterized by a narrower diversity of connectivity configurations, impaired dynamism and lower flexibility, compromising the ability of the networks for a rapid and efficient reorganization of their activity patterns. Remarkably, the altered FC dynamics in our hiPSCs-derived neuronal networks followed the same direction as the resting-state connectivity dynamics observed in the brain of patients with schizophrenia [14].

We observed that resting-state FC in long-term neuronal cultures is a dynamic but not random phenomenon that exhibits recurrent configurations, resembling what has been described in the human brain using fMRI, which characterizes by a much lower spatial and temporal resolution as compared to our *in-vitro* methodology [11]. This observation is consistent with the concept of a “default mode” of neural activity, detected in different brain areas in resting condition, which may contribute to a basal activity state that provides an adequate starting point for efficient response to environmental changes [48]. Hence, addressing the differences and similarities of activity configuration dynamics in resting-state across different spatiotemporal domains, could contribute to understanding the neurobiological bases of brain integration in both health and disease. With this in mind, we explored possible fundamental differences associated with schizophrenia in the dynamics of neuronal network auto-organization, by evaluating FC-related variables in hiPSCs-derived cultures resembling early neurodevelopment. According to our results, schizophrenia networks visited fewer different FC meta-states (MSs), exhibited a reduced number of transitions and spent longer uninterrupted periods of time in the same connectivity configurations, as compared to healthy controls. In addition, the maximum change in a single step that the FC configuration could achieve was reduced in schizophrenia networks, evidencing alterations in FC fast switching associated with schizophrenia. Also, the decreased dynamic range observed in schizophrenia networks suggests that the possibility of

different FC configurations in schizophrenia neuronal networks is more restricted than in healthy control circuits, which is consistent with the lower number of different MSs visited by schizophrenia networks. These early developmental alterations in neural communicational dynamics described in schizophrenia might be jeopardizing the ability of the nervous system for fast and efficient reorganization and converging into a more vulnerable organism to harmful or stressful external factors, leveraging it to schizophrenia development during adulthood [49].

An important observation was the presence of recurrently visited FC MSs (hub MSs) in hiPSCs neuronal networks. Schizophrenia networks showed a reduced repertoire of hub MSs and visited hub MSs less frequently, but remained longer periods of time trapped at the same hub configuration. It has been proposed that long-term potentiation (LTP; a widely studied model of synaptic plasticity) could constitute the neurophysiological basis for the formation of brain hub states [50]. The reduction in the number of hub MSs in schizophrenia networks might be related to an altered plasticity mechanism for reinforcing certain neuronal connections during neurodevelopment, resulting in fewer different configurations strengthened in schizophrenia networks. Actually, genome wide-association studies [51-53] and a recent single-nucleus RNA sequencing analysis of schizophrenia *post-mortem* brain tissue [54], evidenced alterations in the sequence and expression of genes involved in signaling pathways related to plasticity in schizophrenia [55].

Interestingly, the reduction in the number of different hub MSs and total visits to hub MSs displayed by schizophrenia networks, was no longer detected when increasing the width of the time-window to ~30 s (200 frames). An overall decrease in the number of visited MSs was observed while the time-window width was extended (Tables S3-S5). A plausible interpretation of these results may be a progressive reduction in the ability to discriminate some populations of visited MSs when using longer time windows. Presumably, the MSs that could no longer be detected were short-lived connectivity configurations. In this line, a possible explanation for the loss of statistical differences in the number of hub MSs and total visits to hub MSs between schizophrenia and healthy controls, when using the longest time-window, could be that schizophrenia networks have a lower proportion of short-lasting hub MSs compared to healthy controls. Thereby, the percentage of missed events would be smaller in schizophrenia networks as compared to healthy controls when using the longest time-

window, which might have reduced the differences in the number and total visits to hub MSs between the groups. This possibility is consistent with the reduced dynamism of FC in schizophrenia networks. Overall, these results highlight the relevance of improving the time resolution for acquisition and analysis of FC data.

Several genes related to neurodevelopment and synaptic function have been implicated in the pathophysiology of schizophrenia (discussed in [56]). We observed that the expression of genes encoding key glutamatergic postsynaptic proteins presented an altered evolution during early development in schizophrenia networks. The decreased expression of excitatory synaptic components in healthy control neurons along with differentiation contrasted with the rising trend observed in schizophrenia, whereas the expression of the gene encoding the GABAergic synaptic scaffold GEPHYRIN similarly decreased in schizophrenia and in healthy control neurons during differentiation. Taken together, these results suggest an impairment in the excitation/inhibition balance in schizophrenia networks during early development, with a possible trend to develop hyper-excitability. This is consistent with previous observations in patients with schizophrenia [6, 36, 57] and also with transcriptomic analysis of cerebral organoids derived from schizophrenia patients [58]. It could be hypothesized that a shift in the excitation/inhibition balance producing neuronal hyper-excitability might cause the network to approach saturating levels of activity, which might lead to a more restricted set of possible connectivity configurations. This would be consistent with the lower network dynamism observed in schizophrenia networks. However, as we only evaluated the expression of a few synaptic genes, we cannot establish an overall view of the number/activity of potential inhibitory and excitatory synapses in the networks. Instead, we can only estimate, according to the genes we evaluated, that there seems to be a tendency to hyper-excitability in schizophrenia networks.

The observed difference in *ATP5* expression pattern between schizophrenia and healthy control neurons during differentiation might reflect alterations in the cellular metabolism during early developmental stages in schizophrenia. Interestingly, Hahn et al., 2020 [42] described the intimate relationship between brain metabolic demands and FC during cognitive tasks. It would have been informative to evaluate relationships between network gene expression and the measured FC-related variables; however, to collect enough material to quantify gene expression, we pooled cell cultures from

different plates. Therefore, we cannot relate gene expression with functional characterization derived from the same plate.

The expression and activity of CDKR5, and so the activity of CDK5, is tightly regulated and cyclically varies during development and adulthood [38, 59]. According to our data, the reduction in *CDK5R1* expression during neuronal differentiation was less pronounced in schizophrenia networks, as compared to healthy controls, contrasting with *post-mortem* examinations of brain tissue from schizophrenia patients indicating reduced expression of *CDK5R1* as compared to control tissue [60, 61]. Together, these findings may indicate a dysregulation in the upstream molecular mechanisms that control *CDK5R1* expression in schizophrenia, leading to divergences in *CDK5R1* expression throughout development and adulthood.

We are aware that additional factors might be influencing our results and thus it is necessary to be cautious in their interpretation. The main limitation is perhaps the low number of cell lines and replicates used to generate the data. In addition, the incomplete information available on the life history of the donors could be misleading the interpretation of our results, since other covariates might contribute to the differences between the groups. Future experiments including larger samples are crucial to validate our observations in schizophrenia. A technical limitation of our methodology is the arbitrary definition of the focus during calcium imaging. As our cultures were composed of multiple cellular layers of overlapping neurons, the focus election defined the spatial limits of the analyzed networks, which may have influenced the resulting MSs and the inference of FC-related variables.

FC in neuronal cultures has also been evaluated using extracellular microelectrode arrays (MEAs). MEAs allow monitoring of electrical activity at many sites of a network. Nowadays, the development of high-density MEAs allows discrimination of electric signals near the single-cell resolution in cellular cultures [62]. In addition, MEAs recordings exhibit higher temporal resolution than calcium imaging, allowing more precise delineation of the activity transients, and thereby, a more precise estimation of FC. Our analysis designed to quantify FC dynamics could be applied in MEAs data; thereby, the focus limitation inherent to calcium imaging would be improved and the increase in temporal resolution may contribute to identify short-lived connectivity configurations. Furthermore, due to the high temporal resolution achieved with MEAs, point-processes, such as spike trains, can be estimated from the time-serial records

obtained with this technique. In that case, the directionality of FC could be estimated with a cross-correlation analysis, which would allow identifying a greater diversity of connectivity MSs by discriminating between neurons acting either as effectors or receptors of the activity.

Regarding the functional topology of the networks, positive as well as negative correlations were identified, suggesting the influence of excitatory and inhibitory synapses on the diversity of network connectivity patterns. This was supported by the expression of excitatory (*HOMER1* and *GRIN1*), as well as inhibitory (*GPHN* and *GAD67*) synapses marker genes in the networks. However, the slow time course of the calcium transients makes the interpretation of the negative correlation indexes not straightforward, due to possible mono and multi-synaptic influences. Here, we used a similar differentiation procedure as Kirwan et al., 2012 [19], who showed that while GABA-A and B receptors are functional, application of a GABA-A receptor antagonist had no effect on the highly synchronized activity, indicating no significant influence of inhibition on this form of coordinated activity. However, authors did not check the effect of GABA inhibitors in a form of recurrent activity where massive synchronization was less frequent or absent [19], as was the activity presented in our networks. Therefore, the effective participation of inhibitory synapses in the generation of negative correlations in our networks cannot be ruled out and requires further investigation.

Collectively, our findings support previous hypotheses proposing that the brain is a complex system that may possess spatiotemporal scale-invariant principles governing its structure and function through development [63] (discussed in [46, 47]), and add evidence suggesting that these principles are expressed at very early stages of development, when neuronal networks are in an emerging state. Of note, we were able to detect aberrant neural communicational dynamics already in the developing neuronal networks derived from schizophrenia patients that may contribute to the altered FC described in the schizophrenia brain. The integration of our methodology, aiming to evaluate network functional performance, with genome-wide transcriptomic analysis may further contribute to understanding the molecular and cellular mechanisms underlying FC impairments in schizophrenia.

Acknowledgments

We are grateful to Joaquín Cerda for technical support.

Financial support and sponsorship

FONDECYT # 119083 and 1221522 (VP), CONICYT Fellowships for PhD studies # 21181102 (SP), CONICYT/ANID Fellowships for PhD # 21150781 (BC).

Conflicts of interest

The authors declare no conflict of interest.

Availability of supporting data

All the data are available upon request. All proteome membranes are displayed in annexed figures. Raw neural connectivity data along with code that enables analysis and measurement of FC dynamics available at

<https://doi.org/10.5281/zenodo.5130447>

Author contributions

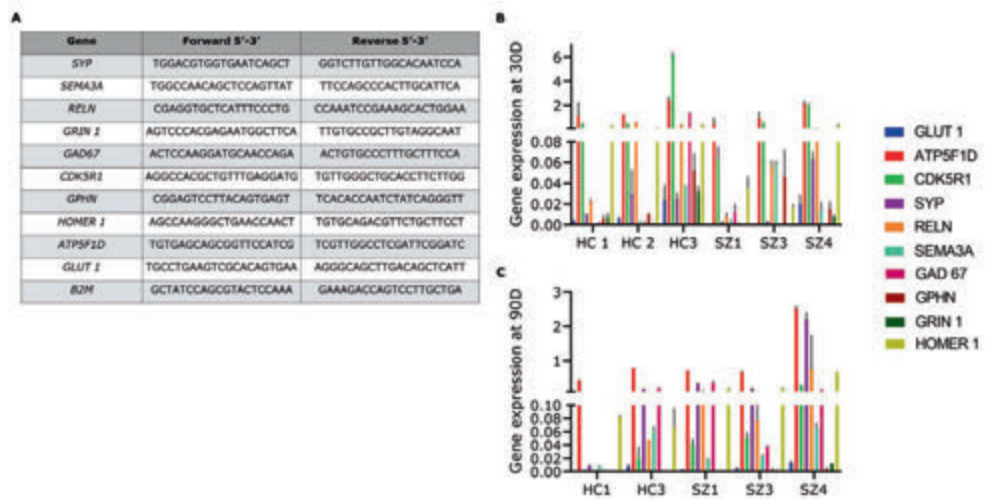
S.P. differentiated the cell cultures in collaboration with B.C., completed imaging experiments, wrote code, analyzed imaging data, implemented the mathematical modeling of *in-vitro* FC dynamics, and wrote the first draft of the manuscript. K.B. built the imaging set-up, designed and participated in the imaging experiments, and calcium transient analysis, and conducted the electrophysiological recordings. R.M., oriented S.P. to adapt her published mathematical methods for whole-brain dynamics to a cellular model and supported with data analysis and interpretation. B.C. and D.G. designed, performed, and analyzed qPCR and proteomic experiments. S.A analyzed the effect of TTX application on the activity of neuronal cultures. S.R generated most of the hiPSCs lines used in the present work and differentiated them to NSCs. All authors actively participated in the interpretation of results and edited and improved the manuscript. M.S. contributed to research design, imaging setup implementation, the guidance of mathematical analysis, and manuscript redaction. Conceptualization, formal analysis writing-review and editing, and general supervision were conducted by V.P.

Supplemental information

Supplementary Table 1. hiPSCs lines used in this study.

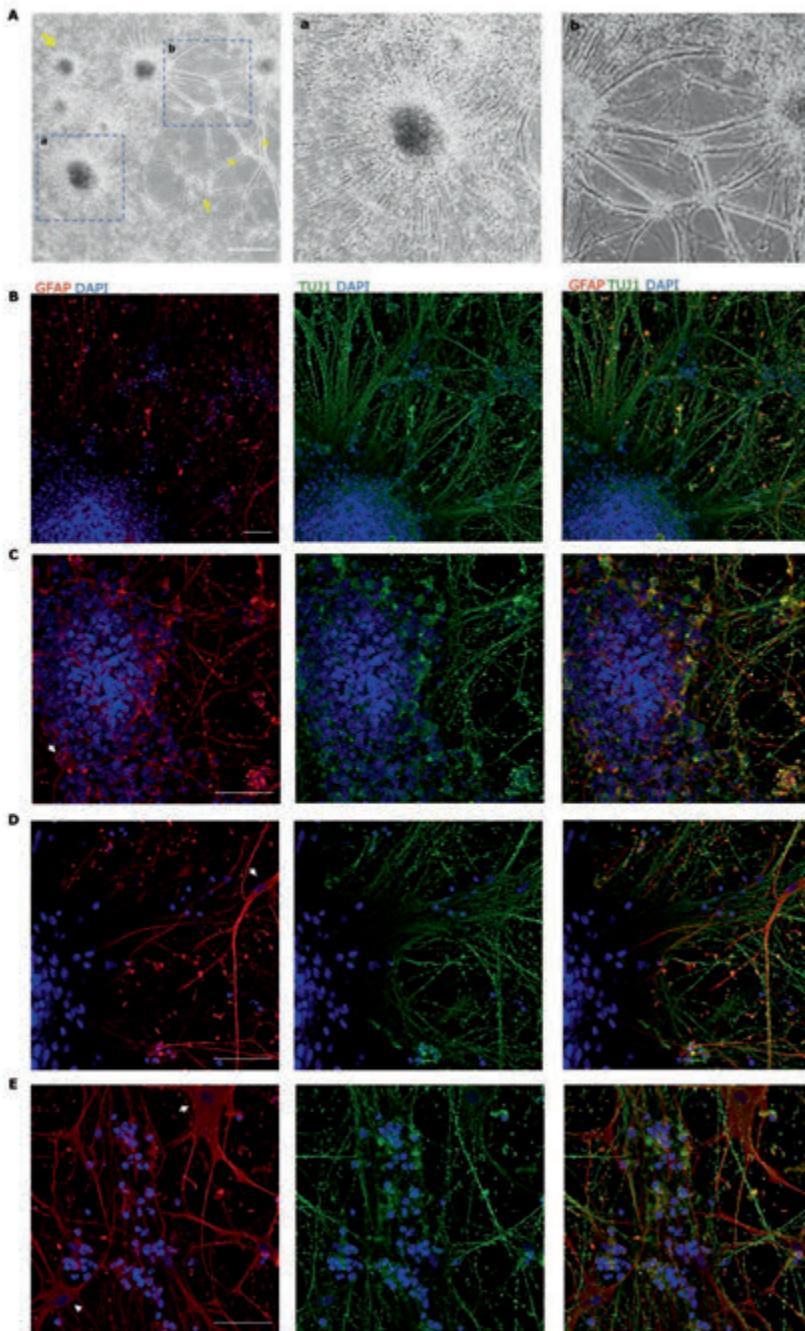
code	cell line	diagnosis	sex	age (range)	cell source	reprogramming technique
HC#1	GM23279A	control	F	36-40	fibroblast	Cytotune 1.0 kit (ThermoFisher)
HC#2	CF2	control	M	31-35	fibroblast	Cytotune 1.0 kit (ThermoFisher)
HC#3	ADHD2	control	M	31-35	urine endothelial	(OCT4, SOX2, KLF4, MYC)
SZ#1	GM23760B	schizophrenia	M	26-30	fibroblast	Cytotune 2.0 kit (ThermoFisher)
SZ#2	GM23761B	schizophrenia	F	26-30	fibroblast	(OCT4, SOX2, KLF4, MYC, LIN28)
SZ#3	EZQ3	schizophrenia	M	41-45	fibroblast	Cytotune 2.0 kit (ThermoFisher)
SZ#4	EZQ4	schizophrenia	M	41-45	fibroblast	(OCT4, SOX2, KLF4, MYC, LIN28)

Information about diagnosis, sex and age of the patients [23, 25]. Schizophrenia (SZ), Healthy control (HC).



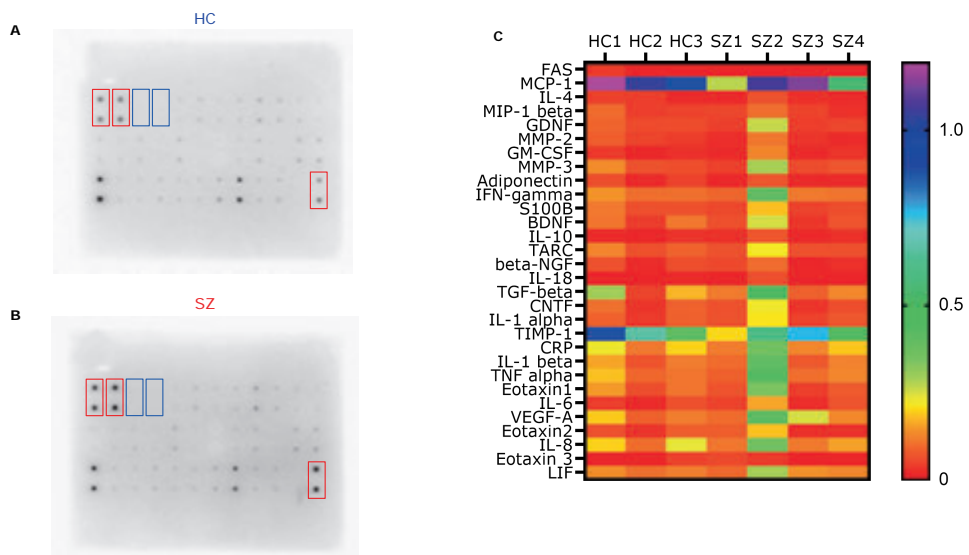
Supplementary Figure 1. qPCR in neuronal cultures at 30 and 70-91 days of differentiation.

(A) Primers used for qPCR amplification. mRNA expression levels of different genes related to nervous system development at 30 (B) and 70-91(C) days of differentiation. *B2M* was used as housekeeping gene. Data are shown as mean \pm standard deviation (SD).



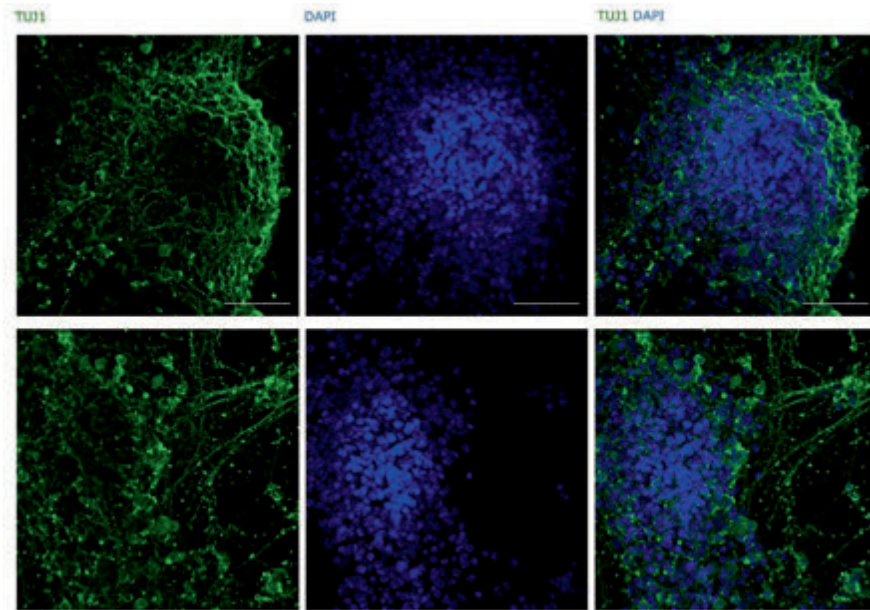
Supplementary Figure 2. Representative images of long-term neuronal cultures at 100 days of differentiation, revealing the presence of astrocytes.

A) Phase contrast image. Arrows indicate 3D neuronal aggregates of different sizes and stars show “bundles” of neuronal projections. Scale bar: 500 μ m. Magnifications of representative neuronal aggregates (a) and neuronal bundles (b) are shown. **(B-E)** Representative images of immunostaining for the astrocyte marker GFAP (red) and neuronal marker TUJ1 (green). Images highlight different structures in the neuronal cultures: **(B)** neuronal aggregates communicating through neuronal bundles at low magnification; **(C)** medium size neuronal aggregates; **(D)** small neuronal aggregates and **(E)** neuronal bundles. Representative astrocytes, covering the bottom of the plate, are indicated with white arrows. Nuclear DAPI staining is shown in blue. Scale bar: 50 μ m.



Supplementary Figure 3. Neurogenic secretome profiling of hiPSCs-derived neuronal cultures.

(A-B) Representative raw data of the neurogenic secretome profile of healthy control and schizophrenia conditioned media. Red boxes indicate positive internal control spots; blue boxes show negative internal control spots. **(C)** Heatmap depicting the levels of neurogenic proteins present in four schizophrenia (#1-4) and three healthy control (#1-3) cell lines at 75 days of differentiation. Data are shown as average level relative to internal control. Schizophrenia (SZ), Healthy control (HC).



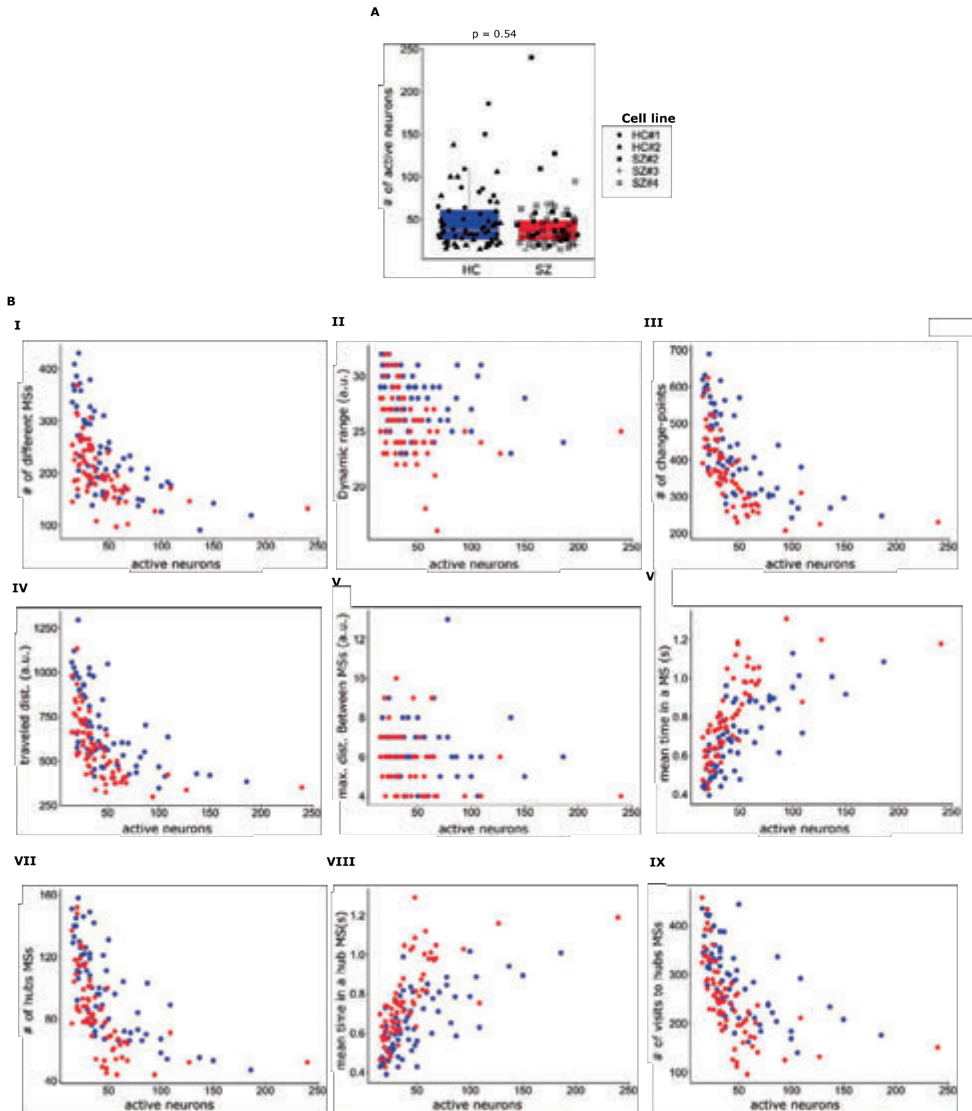
Supplementary Figure 4. Representative images of long-term neuronal cultures at 100 days of differentiation, revealing the presence of axons in neuronal aggregates.

Immunostaining for the neuronal marker TUJ1 (green) in representative neuronal aggregates show the presence of axons in these structures. Nuclear DAPI staining is shown in blue. Scale bar: 50 μm .

Supplementary Table 2. Changes in mRNA expression levels along neuronal differentiation.

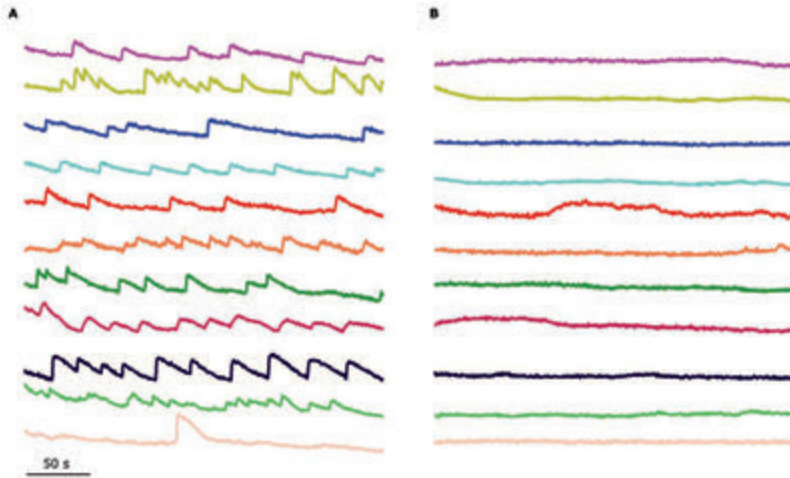
gene	mean log fold-change (90/30 D) in HC networks	fdr adjusted p value	change in HC	mean log fold-change (90/30 D) in SZ networks	fdr adjusted p value	change in SZ
<i>HOMER1</i>	-2.07	4.59×10^{-5}	decrease	2.30	6.35×10^{-4}	increase
<i>GRIN1</i>	-7.36	1.13×10^{-6}	decrease	2.28	1.06×10^{-1}	no change
<i>GPHN</i>	-6.61	2.16×10^{-127}	decrease	-3.37	6.89×10^{-5}	decrease
<i>SYP</i>	1.26	4.49×10^{-1}	no change	NA	NA	NA
<i>CDK5R1</i>	-8.33	5.62×10^{-77}	decrease	-2.38	1.18×10^{-2}	decrease
<i>RELN</i>	4.25	6.03×10^{-2}	no change	-7.55	1.44×10^{-2}	decrease
<i>GAD67</i>	-1.86	7.01×10^{-2}	no change	3.79	1.72×10^{-2}	increase
<i>GLUT1</i>	-3.08	5.57×10^{-2}	no change	2.63	1.33×10^{-1}	no change
<i>SEMA3A</i>	1.81	1.14×10^{-1}	no change	1.10	4.26×10^{-1}	no change
<i>ATP5</i>	-1.51	9.14×10^{-54}	decrease	0.14	6.8×10^{-1}	no change

Changes in mRNA expression levels of different neurodevelopment-related genes between the 30 and 90 days in culture, for healthy control and schizophrenia conditions. We estimated the mean log₂ fold-change in mRNA expression with a unconditional linear model with a random intercept for cell line identity, to account for the variability within the different cell lines (three SZ (#1, 2, and 3) and two HC (#2 and 3)). With the exception of *SYP* in SZ#1, all measurements were performed in duplicates per cell line. The p value associated with the mean is obtained from the z-score of the estimated intercept in the linear regression model. If the mean log fold-change 90/30 is significantly larger than zero, we considered an increase in gene expression and vice-versa. For p value > 0.5, we cannot reject the null hypothesis, suggesting that there was no change in gene expression during the assessed period. Schizophrenia (SZ), Healthy control (HC).



Supplementary Figure 5. FC-related variables correlate with the number of active neurons.

(A) Boxplots indicating the number of active neurons in the networks, in schizophrenia and healthy controls. Each single data is plotted independently on the boxplot and its symbol indicates the cell line of the particular network. There is no difference in the number of active neurons per network between healthy control and schizophrenia condition. **(B)** Scatter plots indicating the relation between the different FC-related variables and the number of active neurons (B.I-B.IX). In most cases, the dependent variable correlated with the number of active neurons in both healthy control and schizophrenia conditions. Schizophrenia (SZ), Healthy control (HC).



Supplementary Figure 6. Ca²⁺ signals rely on voltage-gated Na⁺ channels activation.

Representative Ca²⁺ signals from 11 selected neurons from a neuronal network (**A**). Events are abolished after adding TTX (0.2 μM) to the bath (**B**), confirming the AP-dependence of Ca²⁺ transients.

Supplementary Table 3. Specifications and output of the mixed effect regression models used to quantify the different FC-related variables (width of the sliding time-window used to identify meta-states = 70 frames, 10.5 s).

dependent variable	intercept (average)	estimated SZ effect	p value	optimizer	included predictors	convergence
# of active neurons	49.65	-6.31	5.54×10^{-1}	BFGS	diagnosis, a random intercept per cell line.	yes
# of different MSs	341.95	-51.47	4.43×10^{-3}	CG	diagnosis, # of neurons, # of neurons ² , a random intercept per cell line.	yes
dynamic range (a.u)	29.69	-2.46	1.08×10^{-3}	BFGS	diagnosis, # of neurons, # of neurons ² , a random intercept per cell line.	yes
# of change-points	622.06	-85.38	4.85×10^{-9}	BFGS	diagnosis, # of neurons, # of neurons ² , a random intercept per cell line.	yes
mean time in a MS (frames)	2.12	1.06	2.96×10^{-6}	BFGS	diagnosis, # of neurons, # of neurons ² , a random intercept per cell line.	yes
max. dist. between MSs (a.u)	6.37	-0.69	3.17×10^{-2}	BFGS	diagnosis, a random intercept per cell line.	yes
traveled dist. (a.u)	1044.02	-165.04	8.11×10^{-8}	BFGS	diagnosis, # of neurons, # of neurons ² , a random intercept per cell line.	yes
# of hub MSs	149.57	-22.31	3.1×10^{-6}	CG	diagnosis, # of neurons, # of neurons ² , a random intercept per cell line.	yes
# of visits to hub MSs	430.11	-60.17	5.28×10^{-3}	CG	diagnosis, # of neurons, # of neurons ² , a random intercept per cell line.	yes
mean time in a hub Ms (frames)	2.34	1.11	5.35×10^{-5}	CG	diagnosis, # of neurons, # of neurons ² , a random intercept per cell line.	yes

Schizophrenia effect and *p* value associated with the different variables describing the dynamism of networks functional connectivity (FC), obtained by mixed linear regression modeling (see Methods and Materials). The schizophrenia effect is the coefficient for the diagnosis variable (coded as “1” for schizophrenia and “0” for healthy control networks). The optimizer and predictors used in each regression model are also shown. Schizophrenia (SZ), Healthy control (HC).

Supplementary Table 4. Specifications and output of the mixed effect regression models used to quantify the different FC-related variables (width of the sliding time-window used to identify meta-states = 100 frames, 15.1 s).

dependent variable	intercept (average)	estimated SZ effect	p value	optimizer	included predictors	convergence
# of active neurons	49.66	-6.31	5.54×10^{-1}	BFGS	diagnosis, a random intercept per cell line.	yes
# of different MSs	241.8	-35.8	1.7×10^{-3}	CG	diagnosis, # of neurons, # of neurons ² , a random intercept per cell line.	yes
dynamic range (a.u)	28.78	-2.81	6.76×10^{-5}	BFGS	diagnosis, # of neurons, # of neurons ² , a random intercept per cell line.	no
# of change-points	423.52	-65.62	8.56×10^{-10}	BFGS	diagnosis, # of neurons, # of neurons ² , a random intercept per cell line.	yes
mean time in a MS (frames)	2.97	1.83	4.9×10^{-8}	BFGS	diagnosis, # of neurons, # of neurons ² , a random intercept per cell line.	yes
max. dist. between MSs (a.u)	5.75	-0.75	8.51×10^{-12}	BFGS	diagnosis, a random intercept per cell line.	yes
traveled dist. (a.u)	671.88	-120.90	3.58×10^{-11}	BFGS	diagnosis, # of neurons, # of neurons ² , a random intercept per cell line.	no
# of hub MSs	100	-16.84	1.29×10^{-5}	BFGS	diagnosis, # of neurons, # of neurons ² , a random intercept per cell line.	yes
# of visits to hub MSs	281.84	-47.71	5.71×10^{-9}	CG	diagnosis, # of neurons, # of neurons ² , a random intercept per cell line.	yes
mean time in a hub Ms (frames)	2.84	1.76	2.73×10^{-9}	BFGS	diagnosis, # of neurons, # of neurons ² , a random intercept per cell line.	no

Supplementary Table 5. Specifications and output of the mixed effect regression models used to quantify the different FC-related variables (width of the sliding time-window used to identify meta-states = 200 frames, 30.1 s).

dependent variable	intercept (average)	estimated SZ effect	p value	optimizer	included predictors	convergence
# of active neurons	49.66	-6.31	5.54×10^{-1}	BFGS	diagnosis, a random intercept per cell line.	yes
# of different MSs	111.64	-13.77	2.55×10^{-7}	BFGS	diagnosis, # of neurons, # of neurons ² , a random intercept per cell line.	no
dynamic range (a.u)	25.16	-1.99	5.15×10^{-3}	BFGS	diagnosis, # of neurons, # of neurons ² , a random intercept per cell line.	yes
# of change-points	176.78	-23.88	1.69×10^{-3}	BFGS	diagnosis, # of neurons, # of neurons ² , a random intercept per cell line.	yes
mean time in a MS (frames)	7.66	3.42	6.16×10^{-4}	BFGS	diagnosis, # of neurons, # of neurons ² , a random intercept per cell line.	yes
max. dist. between MSs (a.u)	4.31	-0.47	7.49×10^{-3}	BFGS	diagnosis, a random intercept per cell line.	no
traveled dist. (a.u)	258.21	-41.82	1.82×10^{-4}	BFGS	diagnosis, # of neurons, # of neurons ² , a random intercept per cell line.	yes
# of hub MSs	37.54	-6.03	6.35×10^{-2}	BFGS	diagnosis, # of neurons, # of neurons ² , a random intercept per cell line.	yes
# of visits to hub MSs	103.83	-15.52	1.22×10^{-1}	BFGS	diagnosis, # of neurons, # of neurons ² , a random intercept per cell line.	yes
mean time in a hub Ms (frames)	6.92	3.10	6.04×10^{-3}	BFGS	diagnosis, # of neurons, # of neurons ² , a random intercept per cell line.	yes

References

1. World Health Organization. Mental Disorders 2019, Available from: <https://www.who.int/news-room/fact-sheets/detail/schizophrenia> [Accessed 25 June 2021].
2. Fatemi, S.H. and T.D. Folsom, *The neurodevelopmental hypothesis of schizophrenia, revisited*. Schizophr Bull, 2009. **35**(3): p. 528-48.
3. Fitzsimmons, J., M. Kubicki, and M.E. Shenton, *Review of functional and anatomical brain connectivity findings in schizophrenia*. Curr Opin Psychiatry, 2013. **26**(2): p. 172-87.
4. Schölvinck, M.L., A. Maier, F.Q. Ye, et al., *Neural basis of global resting-state fMRI activity*. Proceedings of the National Academy of Sciences, 2010. **107**(22): p. 10238.
5. Garrity, A.G., G.D. Pearlson, K. McKiernan, et al., *Aberrant "default mode" functional connectivity in schizophrenia*. Am J Psychiatry, 2007. **164**(3): p. 450-7.
6. Whitfield-Gabrieli, S., H.W. Thermenos, S. Milanovic, et al., *Hyperactivity and hyperconnectivity of the default network in schizophrenia and in first-degree relatives of persons with schizophrenia*. Proc Natl Acad Sci U S A, 2009. **106**(4): p. 1279-84.
7. Sheffield, J.M. and D.M. Barch, *Cognition and resting-state functional connectivity in schizophrenia*. Neurosci Biobehav Rev, 2016. **61**: p. 108-20.
8. Erdeniz, B., E. Serin, Y. İbadi, et al., *Decreased functional connectivity in schizophrenia: The relationship between social functioning, social cognition and graph theoretical network measures*. Psychiatry Res Neuroimaging, 2017. **270**: p. 22-31.
9. Godwin, D., A. Ji, S. Kandala, et al., *Functional Connectivity of Cognitive Brain Networks in Schizophrenia during a Working Memory Task*. Front Psychiatry, 2017. **8**: p. 294-294.
10. Menon, S.S. and K. Krishnamurthy, *A Comparison of Static and Dynamic Functional Connectivities for Identifying Subjects and Biological Sex Using Intrinsic Individual Brain Connectivity*. Scientific Reports, 2019. **9**(1): p. 5729.
11. Cabral, J., M.L. Kringelbach, and G. Deco, *Functional connectivity dynamically evolves on multiple time-scales over a static structural connectome: Models and mechanisms*. Neuroimage, 2017. **160**: p. 84-96.
12. Geng, H., P. Xu, I.E. Sommer, et al., *Abnormal dynamic resting-state brain network organization in auditory verbal hallucination*. Brain Struct Funct, 2020. **225**(8): p. 2315-2330.
13. Hutchison, R.M., T. Womelsdorf, E.A. Allen, et al., *Dynamic functional connectivity: promise, issues, and interpretations*. Neuroimage, 2013. **80**: p. 360-78.
14. Miller, R.L., M. Yaesoubi, J.A. Turner, et al., *Higher Dimensional Meta-State Analysis Reveals Reduced Resting fMRI Connectivity Dynamism in Schizophrenia Patients*. PLOS ONE, 2016. **11**(3): p. e0149849.
15. Arthurs, O.J. and S. Boniface, *How well do we understand the neural origins of the fMRI BOLD signal?* Trends in Neurosciences, 2002. **25**(1): p. 27-31.
16. Vadodaria, K.C., J.R. Jones, S. Linker, et al., *Modeling Brain Disorders Using Induced Pluripotent Stem Cells*. Cold Spring Harb Perspect Biol, 2020. **12**(6).
17. Mariani, J., M.V. Simonini, D. Palejev, et al., *Modeling human cortical development in vitro using induced pluripotent stem cells*. Proc Natl Acad Sci U S A, 2012. **109**(31): p. 12770-5.
18. Brennand, K., J.N. Savas, Y. Kim, et al., *Phenotypic differences in hiPSC NPCs derived from patients with schizophrenia*. Molecular psychiatry, 2014. **20**: p. 361.
19. Kirwan, P., B. Turner-Bridger, M. Peter, et al., *Development and function of human cerebral cortex neural networks from pluripotent stem cells in vitro*. Development, 2015. **142**(18): p. 3178-87.
20. Paşca, A.M., S.A. Sloan, L.E. Clarke, et al., *Functional cortical neurons and astrocytes from human pluripotent stem cells in 3D culture*. Nat Methods, 2015. **12**(7): p. 671-8.
21. Izsak, J., H. Seth, M. Andersson, et al., *Robust Generation of Person-Specific, Synchronously Active Neuronal Networks Using Purely Isogenic Human iPSC-3D Neural Aggregate Cultures*. Frontiers in Neurosciences, 2019. **13**(351).
22. Fair, S.R., D. Julian, A.M. Hartlaub, et al., *Electrophysiological Maturation of Cerebral Organoids Correlates with Dynamic Morphological and Cellular Development*. Stem Cell Reports, 2020. **15**(4): p. 855-868.

23. Brennand, K.J., A. Simone, J. Jou, *et al.*, *Modelling schizophrenia using human induced pluripotent stem cells*. *Nature*, 2011. **473**(7346): p. 221-225.
24. Sochacki, J., S. Devalle, M. Reis, *et al.*, *Generation of iPS cell lines from schizophrenia patients using a non-integrative method*. *Stem Cell Research*, 2016. **17**(1): p. 97-101.
25. Casas, B.S., G. Vitória, M.N. do Costa, *et al.*, *hiPSC-derived neural stem cells from patients with schizophrenia induce an impaired angiogenesis*. *Transl Psychiatry*, 2018. **8**(1): p. 48-48.
26. Shi, Y., P. Kirwan, and F.J. Livesey, *Directed differentiation of human pluripotent stem cells to cerebral cortex neurons and neural networks*. *Nat Protoc*, 2012. **7**(10): p. 1836-46.
27. Miura, K., *Bleach correction ImageJ plugin for compensating the photobleaching of time-lapse sequences*. *F1000Res*, 2020. **9**: p. 1494.
28. Giovannucci, A., J. Friedrich, P. Gunn, *et al.*, *CalmAn an open source tool for scalable calcium imaging data analysis*. *Elife*, 2019. **8**.
29. Hyvärinen, A. and E. Oja, *Independent component analysis: algorithms and applications*. *Neural Netw*, 2000. **13**(4-5): p. 411-30.
30. Bahrami, F. and M. Janahmadi, *Antibiotic supplements affect electrophysiological probability and excitability of rat hippocampal pyramidal neurons in primary culture*. *Iran Biomed J*, 2013. **17**(2): p. 101-106.
31. Ryu, A.H., W.L. Eckalbar, A. Kreimer, *et al.*, *Use antibiotics in cell culture with caution: genome-wide identification of antibiotic-induced changes in gene expression and regulation*. *Scientific Reports*, 2017. **7**(1): p. 7533.
32. Xiao, B., J.C. Tu, R.S. Petralia, *et al.*, *Homer Regulates the Association of Group 1 Metabotropic Glutamate Receptors with Multivalent Complexes of Homer-Related, Synaptic Proteins*. *Neuron*, 1998. **21**(4): p. 707-716.
33. Choi, G. and J. Ko, *Gephyrin: a central GABAergic synapse organizer*. *Experimental & Molecular Medicine*, 2015. **47**(4): p. e158-e158.
34. Lau, C.G. and V.N. Murthy, *Activity-dependent regulation of inhibition via GAD67*. *The Journal of neuroscience : the official journal of the Society for Neuroscience*, 2012. **32**(25): p. 8521-8531.
35. Yamamoto, K., T. Kuriu, K. Matsumura, *et al.*, *Multiple alterations in glutamatergic transmission and dopamine D2 receptor splicing in induced pluripotent stem cell-derived neurons from patients with familial schizophrenia*. *Translational Psychiatry*, 2021. **11**(1): p. 548.
36. Allen, P., I.E. Sommer, R. Jardri, *et al.*, *Extrinsic and default mode networks in psychiatric conditions: Relationship to excitatory-inhibitory transmitter balance and early trauma*. *Neurosci Biobehav Rev*, 2019. **99**: p. 90-100.
37. Ko, J., S. Humbert, R.T. Bronson, *et al.*, *p35 and p39 are essential for cyclin-dependent kinase 5 function during neurodevelopment*. *J Neurosci*, 2001. **21**(17): p. 6758-71.
38. Nguyen, M.D., W.E. Mushynski, and J.P. Julien, *Cycling at the interface between neurodevelopment and neurodegeneration*. *Cell Death Differ*, 2002. **9**(12): p. 1294-306.
39. Wu, D.C., Y.P. Yu, N.T. Lee, *et al.*, *The expression of Cdk5, p35, p39, and Cdk5 kinase activity in developing, adult, and aged rat brains*. *Neurochem Res*, 2000. **25**(7): p. 923-9.
40. Wasser, C.R. and J. Herz, *Reelin: Neurodevelopmental Architect and Homeostatic Regulator of Excitatory Synapses*. *J Biol Chem*, 2017. **292**(4): p. 1330-1338.
41. Kumar, A., V. Pareek, H.N. Singh, *et al.*, *Altered Expression of a Unique Set of Genes Reveals Complex Etiology of Schizophrenia*. *Frontiers in Psychiatry*, 2019. **10**(906).
42. Hahn, A., M. Breakspear, L. Rischka, *et al.*, *Reconfiguration of functional brain networks and metabolic cost converge during task performance*. *Elife*, 2020. **9**.
43. Ali, F. and A.C. Kwan, *Interpreting in vivo calcium signals from neuronal cell bodies, axons, and dendrites: a review*. *Neurophotonics*, 2020. **7**(1): p. 011402-011402.
44. in *Jasper's Basic Mechanisms of the Epilepsies*, J.L. Noebels, *et al.*, Editors. 2012, National Center for Biotechnology Information (US) Copyright © 2012, Michael A Rogawski, Antonio V Delgado-Escueta, Jeffrey L Noebels, Massimo Avoli and Richard W Olsen.: Bethesda (MD).

45. Brennand, K.J., A. Simone, J. Jou, *et al.*, *Modelling schizophrenia using human induced pluripotent stem cells*. *Nature*, 2011. **473**(7346): p. 221-5.
46. Bullmore, E. and O. Sporns, *Complex brain networks: graph theoretical analysis of structural and functional systems*. *Nature Reviews Neuroscience*, 2009. **10**(3): p. 186-198.
47. Zhang, J., L. Xu, and Z. Cui, *Convergent developmental principles between *Caenorhabditis elegans* and human connectomes*. *Trends Cogn Sci*, 2021. **25**(12): p. 1015-1017.
48. Raichle, M.E. and A.Z. Snyder, *A default mode of brain function: A brief history of an evolving idea*. *NeuroImage*, 2007. **37**(4): p. 1083-1090.
49. Maynard, T.M., L. Sikich, J.A. Lieberman, *et al.*, *Neural development, cell-cell signaling, and the "two-hit" hypothesis of schizophrenia*. *Schizophr Bull*, 2001. **27**(3): p. 457-76.
50. Stampanoni Bassi, M., E. Iezzi, L. Gilio, *et al.*, *Synaptic Plasticity Shapes Brain Connectivity: Implications for Network Topology*. *International Journal of Molecular Sciences*, 2019. **20**(24): p. 6193.
51. Kirov, G., A.J. Pocklington, P. Holmans, *et al.*, *De novo CNV analysis implicates specific abnormalities of postsynaptic signalling complexes in the pathogenesis of schizophrenia*. *Molecular Psychiatry*, 2012. **17**(2): p. 142-153.
52. Fromer, M., A.J. Pocklington, D.H. Kavanagh, *et al.*, *De novo mutations in schizophrenia implicate synaptic networks*. *Nature*, 2014. **506**(7487): p. 179-84.
53. Purcell, S.M., J.L. Moran, M. Fromer, *et al.*, *A polygenic burden of rare disruptive mutations in schizophrenia*. *Nature*, 2014. **506**(7487): p. 185-90.
54. Batiuk, M.Y., T. Tyler, S. Mei, *et al.*, *Selective vulnerability of supragranular layer neurons in schizophrenia*. *bioRxiv*, 2020: p. 2020.11.17.386458.
55. Hall, J., S. Trent, K.L. Thomas, *et al.*, *Genetic Risk for Schizophrenia: Convergence on Synaptic Pathways Involved in Plasticity*. *Biological Psychiatry*, 2015. **77**(1): p. 52-58.
56. Birnbaum, R. and D.R. Weinberger, *Genetic insights into the neurodevelopmental origins of schizophrenia*. *Nature Reviews Neuroscience*, 2017. **18**(12): p. 727-740.
57. McHugo, M., P. Talati, K. Armstrong, *et al.*, *Hyperactivity and Reduced Activation of Anterior Hippocampus in Early Psychosis*. *Am J Psychiatry*, 2019. **176**(12): p. 1030-1038.
58. Kathuria, A., K. Lopez-Lengowski, S.S. Jagtap, *et al.*, *Transcriptomic Landscape and Functional Characterization of Induced Pluripotent Stem Cell-Derived Cerebral Organoids in Schizophrenia*. *JAMA Psychiatry*, 2020. **77**(7): p. 745-754.
59. Delalle, I., P.G. Bhide, V.S. Caviness, Jr., *et al.*, *Temporal and spatial patterns of expression of p35, a regulatory subunit of cyclin-dependent kinase 5, in the nervous system of the mouse*. *J Neurocytol*, 1997. **26**(5): p. 283-96.
60. Engmann, O., T. Hortobágyi, R. Pidsley, *et al.*, *Schizophrenia is associated with dysregulation of a Cdk5 activator that regulates synaptic protein expression and cognition*. *Brain : a journal of neurology*, 2011. **134**(Pt 8): p. 2408-2421.
61. Ramos-Miguel, A., J.J. Meana, and J.A. García-Sevilla, *Cyclin-dependent kinase-5 and p35/p25 activators in schizophrenia and major depression prefrontal cortex: basal contents and effects of psychotropic medications*. *Int J Neuropsychopharmacol*, 2013. **16**(3): p. 683-9.
62. Poli, D., V.P. Pastore, and P. Massobrio, *Functional connectivity in in vitro neuronal assemblies*. *Front Neural Circuits*, 2015. **9**: p. 57.
63. Witvliet, D., B. Mulcahy, J.K. Mitchell, *et al.*, *Connectomes across development reveal principles of brain maturation*. *Nature*, 2021. **596**(7871): p. 257-261.

